This document is the author accepted manuscript (AAM) version of the work identified by the DOI: 10.1016/B978-0-323-90614-2.00002-X and published in its final form after formatting and technical copy-editing by the publisher as a chapter of the book *Fundamentals and Applications of Nonlinear Nanophotonics*, ed. Nicolae-Coriolan Panoiu, Elsevier (Amsterdam) 2024.

Chapter: Photon management in harmonic generation at the nanoscale

Davide Rocco[1,2], Andrea Tognazzi[1,2], Marco Gandolfi[2,1], Carlo Gigli[3], Attilio Zilli[4], Luca Carletti[1,2], Andrea Locatelli[1,2], Giuseppe Leo[3], Giuseppe Della Valle[4], Marco Finazzi[4], Michele Celebrano[4], Costantino De Angelis[1,2]

[1]Dipartimento di Ingegneria dell'Informazione, Università di Brescia, Via Branze 38 - 25123, Brescia, Italy
[2]Istituto Nazionale di Ottica, Consiglio Nazionale delle Ricerche, Via Branze 45 - 25123, Brescia, Italy
[3]Matériaux et Phénomènes Quantiques, Université de Paris, 10 rue Alice Domon et Léonie Duquet, 75013 Paris, France
[4]Dipartimento di Fisica - Politecnico di Milano, Piazza Leonardo da Vinci, 32 -20133 Milano, Italy

Keywords: second harmonic generation, tunable metasurface, thermo-optical devices, dielectric nanoantennas, reconfigurability

Abstract: Dielectric nanoantennas have recently shown huge potential for nonlinear optics. High-refractive index nano-resonators have proved efficient Second-Harmonic Generation (SHG) and Third-Harmonic Generation (THG) from an optical pump beam either at visible or NIR frequencies in the static regime. In this chapter a focus about SHG in such structures is reported and after a brief historical review of SHG in AlGaAs nanostructures, we report the new promising concept of tunability. In particular, we present two innovative approaches to modulate the nonlinear emission. Firstly, we explain the possibility to modulate the SHG by using liquid crystals and lastly we discuss the thermo-optical modulation of the second harmonic light.

1. Introduction

Nonlinear nanophotonics has recently attracted enormous interest for light-based technologies with potential applications ranging from light sources, tunable components and ultrafast metadevices [1] [2] [3] [4]. Nanoscale-designed components do certainly integrate different functionalities in nanophotonics circuits by improving miniaturization and allowing the replacement of bulky components [5] [6] [7]. One key asset in nonlinear nanophotonics is the capability to achieve strong light–matter interaction through optical resonances in subwavelength nanostructures [8] [9]. Differently from bulk macroscopic media, where the efficiency of nonlinear optical phenomena is mainly determined by intrinsic nonlinear properties and phase-matching conditions, in nonlinear nanophotonics the key challenge is to engineer the nonlinear scattering from nanoscale elements by molding the local electromagnetic field to achieve the desired behavior. Since the nonlinear response strongly depends on localized resonant effects in nanostructures, both modal and multipolar control of the nonlinear response are extensively exploited for boosting the near-field interaction and designing the radiation directionality [10]. The nano-elements, also known as nano-antennas, are typically made of metallic or dielectric materials.

Plasmonic (i.e. gold and silver) nano-structures have been considered at first for enhancing the harmonic generation processes at the nanoscale [11] [12] [13] [14]. Indeed, despite the high absorption losses that affects these materials in the Near Infra-Red (NIR) region [15], plasmonic structures can enhance and confine the electromagnetic radiations in very small volumes. When pumping at moderate pump intensities the high absorption is translated into a sizable heating of the nanoelements, which is a drawback for a diversity of implementations. Especially for sensing applications, small changes in the environmental conditions (such as the temperature) can dramatically affect the final measurements. Indeed, the important temperature increase due to the intrinsic ohmich losses in the system may trigger unwanted chemical reactions or altering the analytes. Another main limitation in terms of total harmonic efficiency of nonlinear metallic-based nano-devices is that they cannot manifest second order nonlinearties from the bulk (due to symmetry reasons) and in general they mainly resort to surface nonlinear susceptibility, which is the dominant component in plasmonic elements since the field cannot penetrate the metal alloys [16].

An alternative to plasmonic structures is represented by dielectric nano-antennas made of high refractive index materials [17] [18]. Dielectric structures have the advantage of negligible losses in the NIR and a dominant bulk contribution as the source of the nonlinearities. Indeed, in dielectrics, the electromagnetic radiation penetrates inside the volume of the nano-element. Typically, the size of the dielectric-based nano-devices is larger and the latter have lower electric field enhancement compared to their plasmonic counterpart, but high refractive index devices offer the possibility to easily access to magnetic resonances, contrary to plasmonic materials that are dominated by electric ones

[19]. Real magnetism in its conventional sense (i.e. from the bulk) is not accessible at high optical frequencies, however, in nanostructured media, it is possible to design the spatial dispersion and electric effects to produce a magnetic dipole moment although the involved materials do not possess microscopic magnetization.

Recently, dielectric nano-antennas have demonstrated enhanced Second-Harmonic Generation (SHG) and Third-Harmonic Generation (THG) from an optical pump beam either at visible or NIR frequencies [20] [21] [22] [23]. Concerning SH processes, as anticipated, this is reached for three main reasons: *i*) the material transparency at both pump and emission frequency; *ii*) the high nonlinear susceptibility; *iii*) the possibility to sustain also magnetic resonances. The enhancement of the harmonic conversion efficiency can be obtained by increasing the coupling between the pump beam and the nano-antenna resonant mode and maximizing the quality (Q) factor of the resonance at the Fundamental Wavelength, FW. Hence, the design of nanoparticles for boosted harmonic generation relies on the study of their linear optical peculiarities such as field enhancement, resonant frequencies, bandwidth, radiation diagrams at fundamental and harmonic frequencies. The optimization of the nanoparticle shape is an important aspect for increasing the overall efficiency. In this context, multipole decomposition of the electric fields and currents is widely adopted due to the close link with the observed physical features [24]. Moreover, in dielectrics, the interaction between electric and magnetic Mie-type resonances can be translated into a relatively high resonant enhancement of electromagnetic fields in the nanostructures, enabling in this way new possibilities for efficient nonlinear processes [25] [26]. More recently, dielectric nanodevices have shown the capability to sustain toroidal resonances (a class of electromagnetic excitation that has recently gained attention in the field of metamaterials [27]), which are useful for exciting radiation-less field distributions also called anapoles [28]. At the anapole condition the electromagnetic field is maximized inside the structure volume and this could be beneficial for nonlinear optics [29]. Following the same approach of maximizing the electric field enhancement inside the high-refractive index resonators, it has been demonstrated that properly designed dielectric nanoparticles support localized states with high-Q factor. This is possible if the geometrical parameters are optimized to obtain a quasi-bound state in the continuum (BIC) formed via destructive interference of two similar leaky modes [30]. Hence, dielectric nanoparticles can exhibit high-Q resonances associated with the so-called super-cavity modes and these large Q factors strongly boost nonlinear effects at the nanoscale. Let us mention that more sophisticated hybrid metal/dielectric approaches have also been proposed, in which one can take advantage of the dielectric bulk nonlinearities and of the higher plasmonic electric field confinement to boost the harmonic generation [31, 32]. Moreover, the so called epsilon-near-zero (ENZ) metamaterials have been proposed for enhancing the nonlinear effects at the nanoscale [33]. The permittivity can be tuned using nanoparticle resonances, which makes the ENZ condition itself relatively simple to fulfill in a composite material. A conventional configuration with a straightforward fabrication procedure is a metal–dielectric stack. Among all the fabricated design, let us mention that a broadband enhancement of the radiated second-harmonic intensity has been demonstrated in hyperbolic gold nanorod metamaterial slab due to the overlap of fundamental and harmonic modes [34].

Indeed, nonlinear devices are usually designed to work in stationary condition, i.e. operating at a fixed wavelength and in a given environment. However, for many applications it is crucial to be able to dynamically tune the optical properties (i.e. optical reconfigurability). In the linear regime, different solutions to access optical reconfigurability have been theoretically and experimentally demonstrated by different research groups; these include mechanical movement of elements; photo- and electro-excitation of free carriers; phase-change materials; and liquid crystal (LC) infiltration [35] [36] [37] [38] [39] [40] [41] [42] [43] [44] [45] [46] [47]. The tunability of the harmonic generated light at the nanoscale has received only recently a great attention in the photonic community working with nanoantennas and metamaterials. For instance, the potential of ENZ materials has been exploited for achieving efficient adiabatic frequency conversion (i.e. a time-dependent change in the refractive index of a material leads to a change in the frequency of an optical beam passing through that medium) in a nonlinear ENZ-based metasurface [48]. Anyhow, the newly achievements regarding reconfigurable nonlinear dielectric metasurfaces is the main topic we want to cover here.

In this chapter, after a brief historical review of SHG in AlGaAs nanostructures and metasurfaces (2D arrangement of nanostructures) in Section 2, we address the new concept of tunability. In particular, we present two promising approaches to modulate the nonlinear emission. In section 3, we will discuss the possibility to tune the SHG by using liquid crystals (mechanically, electrically or optically controlled). In section 4, we will deal with the possibility of thermo-optical modulation of the second harmonic light. Section 5 is devoted to perspectives. The chapter ends with a section dedicated to conclusions.

2. SHG in AlGaAs nanostructures and metasurfaces

Linear optics provides a complete description of light–matter interaction only in the limit of weak radiation sources. When more powerful radiation excitations are considered, the phenomenology of light–matter interaction becomes more complex; as opposed to linear optics, where we often have well-known tools to tackle a specific problem, when nonlinearity comes into play, and the whole can be more than the sum of its parts, we can seldom resort to standard approaches. The emergence of qualitatively new phenomena is offering incredible outcomes for basic and applied sciences [49]. Typically, the induced polarization P can be expressed as a sum:

$$P = P_L + P_{NL} \tag{1}$$

where P_L is the linear part of the electric dipole polarization volume density and P_{NL} represents the nonlinear one. The linear polarization is responsible for linear optical phenomena, namely the regime where the optical properties of a medium are independent of the field intensity. The relation between P_L and the electric field E is given, in the frequency domain, by the standard formula of linear optics:

$$P_L(\omega) = \varepsilon_0 \sum_j \chi_{ij}^{(1)}(\omega) E_j(\omega) \tag{2}$$

where $\chi_{ij}^{(1)}$ is the linear optical susceptibility of the medium and ε_0 is the permittivity of vacuum. In the regime of weak fields, the nonlinear part of the polarization P_{NL} can be represented as a power-series expansion in the field E as: $P_{NL}(\omega) = P^2(\omega) + P^3(\omega) + \cdots$ where:

$$P^{(2)}(\omega) = \varepsilon_0 \sum_{jk} \chi_{ijk}^{(2)}(\omega;\ \omega_m, \omega_n) E_j(\omega_m) E_k(\omega_n), \tag{3}$$

$$P^{(3)}(\omega) = \varepsilon_0 \sum_{jkl} \chi_{ijkl}^{(3)}(\omega;\ \omega_m, \omega_n, \omega_p) E_j(\omega_m) E_k(\omega_n) E_l(\omega_p). \tag{4}$$

The quantities $\chi_{ijk}^{(2)}$ and $\chi_{ijkl}^{(3)}$ are known as the second- and third-order nonlinear optical susceptibility tensor, respectively. In particular, setting $\omega_m = \omega_n = \omega_0$ in (3), we obtain $\omega = 2\omega_0$, that corresponds to second-harmonic generation, governed by the nonlinear susceptibility $\chi_{SHG}^{(2)} = \chi_{ijk}^{(2)}(2\omega_0; \omega_0, \omega_0)$. Instead, for the case of third-harmonic generation, we set $\omega_m = \omega_n = \omega_p = \omega_0$ in (4) to arrive at $\omega = 3\omega_0$. This type of nonlinear-optical interaction is guided by the cubic susceptibility $\chi_{THG}^{(3)} = \chi_{ijkl}^{(3)}(3\omega_0; \omega_0, \omega_0, \omega_0)$. Since the efficiency of a nonlinear phenomenon decreases with increasing nonlinearity order, they represent the two major elastic contributions among the nonlinear optical processes.

Recently, nano-antennas made of high-refractive index resonators have attracted much attention for the nonlinear generation of light, due to their much lower loss compared with their metallic counterparts. At first, Third-Harmonic Generation (THG) in silicon and germanium nano-structures has been investigated, showing an enhanced conversion efficiency by optical pumping in the vicinity of the antenna's magnetic dipole or anapole resonances [26] [50] [51]. More precisely, conversion efficiencies of 10^{-7} and 10^{-6} have been estimated for peak pump intensity of few GW/cm^2 [2] [4] [52] [53] [54]. In this context, the nonlinear efficiency is commonly defined as the emitted nonlinear power divided by the power of the incident beam at the fundamental wavelength. The normalized nonlinear efficiency is instead calculated by dividing the emitted nonlinear power for the square (in the case of SHG) or the third power (THG experiments) of the input power beam, leading in this way to a definition of efficiency that is independent on the excitation properties (average power, pulse duration and repetition rate) and therefore it is expressed in W^{-1} (for SHG processes) or W^{-2} (for THG). The aforementioned spectacular achievements are related to third-order nonlinear effects since silicon and germanium have null bulk quadratic optical nonlinearity in the dipole limit due to their centro-symmetric crystal structure. However, exploiting III–V compounds and alloys with large $\chi^{(2)}$, such as GaP, GaAs and AlGaAs, would intrinsically increase the conversion efficiency due to their lower-order nonlinearity. The nonlinear effects in AlGaAs/GaAs nano-structures have been the subject of continuing research, including SHG in GaAs nanowires, hybrid GaAs plasmonic nano-holes, GaAs micro-ring resonators on insulator and most recently, dielectric nano-antennas and metasurfaces [32] [55] [56] [57] [58]. In particular, $Al_xGa_{1-x}As$ is commonly used in high-speed electronics and opto-electronic devices and is also a medium for integrated nonlinear optics [59] [60] [61]. The success of this material is mainly related to the dependence of the band-gap energy on the alloy composition [62]. A band gap is an energy range in a solid where no electron states can exist. In general, in semiconductors, the band gap corresponds to the minimum energy required to promote a valence electron bound to an atom into the conduction band, where the electron is free to move within the crystal. The band gap is referred to be direct if the transition from the top of the valence band to the bottom of the conduction band can take place without any change of electron momentum . Importantly, $Al_xGa_{1-x}As$ exhibits a direct gap which increases with the Al molar fraction x and allows two-photon-absorption-free operation around the third communication window (~ 1.5μm) when $x \geq 0.18$. Moreover,

AlGaAs possess a large non-resonant quadratic susceptibility ($\chi^{(2)} \approx 200$ pm/V for $Al_{0.18}Ga_{0.82}As$ in the near infrared) [63] [64] [65]. For all these reasons, in the following, we will focus on recent achievements in AlGaAs-based nano-platforms.

Several approaches have been recently proposed for maximizing the efficiency of SHG in AlGaAs nanostructures. Apart from fully theoretical works, where the geometry and the environmental conditions can be easily selected as preferred, when facing the experimental and fabrication state of art, some limitations must be considered. For instance, it is quite easy and stable to fabricate cylindrical nanoantennas (layered over a dielectric substrate with smaller refractive index) through e-beam lithography. At the same time, an experiment involving only normally incident pumps is typically preferred than tilted incident pumps with a large angle of incidence [66]. An aspect to underline is that the total SH efficiency inside the particle grows linearly with the Q-factor of the fundamental excited resonance. Indeed, it has been shown that the total harmonic efficiency coming from nanoparticle is proportional to the product of the so-called coupling efficiency and the resonant response of the resonator. This holds because, despite it is hard to couple the incident energy to modes high Q-factor (the coupling efficiency of the incident energy to the resonator is proportional to Q^{-1}), in the SHG process the resonant enhancement dominates (because the resonant response of the resonator can be estimated to be proportional to Q^2) [30]. With these considerations in mind, we report in the following the recent results related to SHG in AlGaAs nanoantennas. All these achievements go in the direction of maximizing the SHG efficiency by minimizing the fabrication and experimental complexity procedures as much as possible. We also emphasize that SHG efficiency is by no means the solely parameter to look at. Some recent studies have shown that the SH phase plays a crucial role for obtaining nonlinear metasurfaces acting as a metalens or with sizable nonlinear beam steering performance, thus enhancing the potential applications of AlGaAs meta-devices [67].

One of the first reports of the huge potential of AlGaAs for nonlinear nanophotonics appeared in 2015 (Carletti et al [68]); in this theoretical work, SHG efficiency up to 10^{-3} was predicted for a free standing AlGaAs nanocylinder in a homogeneous air environment, using a fundamental wavelength of 1550 nm tuned to the magnetic dipolar resonance of the nanoantenna (pump intensity of 1 GW/cm^2). For this geometry (radius of 225 nm and height of 400 nm), the magnetic dipolar contribution enhances the scattering efficiency at the fundamental wavelength. Notably, AlGaAs belongs to the *3m* symmetry group, and it has a cubic crystalline structure. For such kind of materials, the second-order nonlinear susceptibility tensor has terms different from zero of the type $\chi^{(2)}_{ijk}$ where $i \neq j \neq k$ are crystalline axes. Applying the Kleinman symmetry condition and utilizing the 3×6 d matrix formalism, the only nonvanishing element is d_{36}, which for AlGaAs is 50 pm/V [69]. Hence, the nonlinear currents at the SH frequency can be written as:

$$J_i^{SH} = i\omega_{SH} 4\varepsilon_0 d_{36} E_j^{\omega} E_k^{\omega} \tag{5}$$

where ε_0 is the dielectric permittivity of vacuum, ω_{SH} is the SH angular frequency, and $E_{j(k)}$ is the $j(k)$ Cartesian component of the electric field at the pump frequency ω, with $i \neq j \neq k$. Implementing such currents as optical sources for the numerical simulations at the *SH* frequency, and assuming an undepleted pump regime, in [68] it is possible to compute the SH signal emitted by AlGaAs nanocylinders.

An experimental verification soon followed [66]. In the experiment, AlGaAs nanodisk is supported by a dielectric substrate, which causes a reduction of the collected SH efficiency down to 10^{-5}. Still, this value is orders of magnitude larger than the record SH efficiency achieved in plasmonic nanostructures [70]. Despite the higher losses a further confirmation of enhanced SHG by semiconductor nanoresonators came also from GaAs platform [71].Thus, these encouraging results have pushed the scientific community to find ways to further boost the SHG efficiency. A possible solution that has been proposed is the use of the so-called anapole distributions. [28]. Differently from the magnetic dipolar resonance, that is characterized by a maximum in scattering efficiency of the AlGaAs nanodisk antenna, the anapole condition is associated with null scattering in the far-field together with a maximum of the internal energy inside the dielectric volume. The confinement of the electromagnetic field at the fundamental wavelength can thus boost the SHG. More precisely, the electric anapole is defined as the condition where the electric dipolar and the toroidal dipolar resonances are the dominant excited multipolar contributions with the same amplitude and a π phase shift. Since this two multipoles have the same radiation pattern, they therefore destructively interfere in the far field, thus bringing about the null scattering mentioned above. In [72] the electric anapole has been exploited in a dimer configuration that consists of two AlGaAs nanodisks with a small gap in between. The latter structure not only offers the possibility to boost the SHG efficiency by fulfilling the anapole mode in each nanodisk that form the dimer, but also demonstrates that proper near-field coupling can provide further degrees of freedom to control the polarization state and the radiation diagram of the SHG field. Alternatively, also a hybrid (dielectric and plasmonic) approach has been proposed [31]. For instance, a single AlGaAs nanodisk has been encircled with a surrounding gold nanoring to assist the excitation of the anapole. The SHG efficiency in any case is similar to the one obtained exciting the magnetic dipolar resonance in the isolated AlGaAs nanocylinder. The main reason is that low-order multipolar Mie contributions and anapoles have relatively low Q. Moreover, the electric field inside the resonator is confined in localized hotspots, therefore not all the volume of the structure is efficient in the harmonic generation process.

Exploiting the concept of bound states in the continuum (BIC), more recently, dielectric nanoparticles have been shown to sustain modes with extreme Q [30]. A BIC is a solution of the scattering problem that remains localized despite coexisting with a continuous of radiating waves that can carry energy away; their existence requires either structures extending to infinity in at least one direction or hard walls that spatially separate them from extended states [73]. In this framework, it has been shown that also an individual AlGaAs nanodisk can sustain high Q-factor supercavity modes caused by interference of two similar leaky modes. This phenomenon, which is inspired by the BIC physics, is today referred to as quasi- BIC [74]. In [30] it has been demonstrated a tremendous enhancement of SHG when the resonator (an AlGaAs nanocylinder) parameters are tuned to the quasi-BIC regime. The obtained extremely high normalized conversion efficiency (~10^{-2} W^{-1}) exceeds by 2 orders of magnitude the largest one at the nanoscale demonstrated when a magnetic dipolar resonance is excited at the fundamental wavelength [30]. Figure 1 summarizes the main results in terms of SHG efficiency by exploiting different excited modes at the pump frequency.

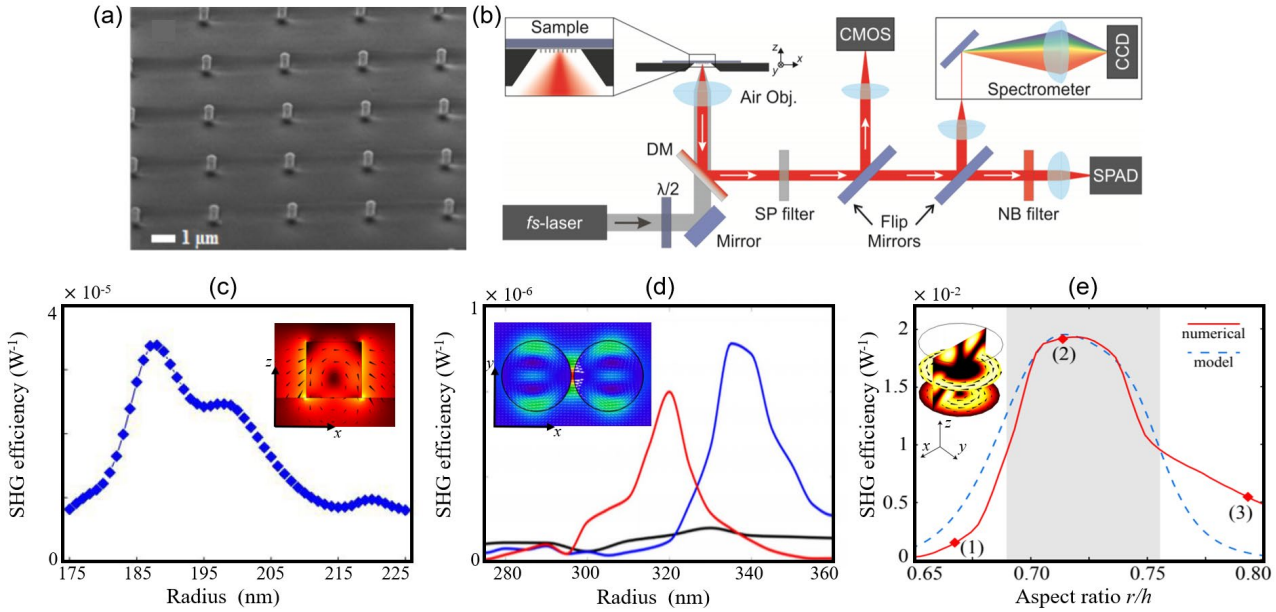

Figure 1. (a) SEM image of a typical fabricated AlGaAs- on- AlOx metasurface composed of cylindrical nano-elements. (b) Experimental set-up for nonlinear micro-spectroscopy of individual nanoantennas. fs-laser: 1554 nm laser delivering 150fs pulses (light grey beam). λ/2: half-wave plate; Air Obj.: 0.85-NA air objective; DM: dichroic mirror; SP & NB filters: short-pass and narrow-band filter. CMOS: imaging camera; SPAD: single-photon avalanche diode; CCD: cooled charge-couple device camera. The sample is mounted facing the objective as depicted in the inset. (c) Numerical calculations of the nanoantenna SHG normalized efficiency as a function of the pillar radius when exciting a MD resonance at the FW. The pillar height is 400 nm. The inset represents the field at 1554 nm (i.e., at FW). Adapted with permission from [66] © The Optical Society. (d) Numerical calculations of the dimer SHG normalized efficiency for x- (blue line) and y- (red line) polarized pump beam as a function of cylinder radius compared to the SHG normalized efficiency of the single cylinder (black line). At the FW the anapole condition is excited as indicated in the inset, in which the E-field is plotted in the case of x-polarized light. The pillar height is 400 nm. Adapted from [72]. (e) SHG normalized efficiency as a function of the nanoparticle aspect ratio r/h calculated by nonlinear simulations in COMSOL (red solid line) and analytically (blue dashed line). Gray area represents the fullwidth-at-half-maximum band of the calculated SHG conversion efficiency. Reprinted figures with permission from [29]. Copyright 2021 by the American Physical Society, https://doi.org/10.1103/PhysRevLett.121.033903.

All the aforementioned cases focus on maximizing the SH efficiency. However, the nonlinear SH emission from an AlGaAs nanodisk (with canonical crystalline axis) is radiated at large angles with respect to the normal direction, representing a serious drawback in practical applications [75]. To overcome such complication, various research groups have proposed to break the symmetry of the system by tilting the pump at an angle or by fabricating AlGaAs nanodisks with crystalline axis rotated with respect to the sample coordinate system by implementing epitaxial growth on either (111) or (110) substrates [76] [20]. However, the latter approach is not easy to pursue because it demands for higher growth temperatures, thus typically leading to an irregular morphology. Moreover, both (111) and (110) substrates are not standard in diode laser technology and reduce the compatibility of the related meta-structures in view of optoelectronic integration. Instead, a valuable solution has been recently proposed in [77], where an asymmetrical AlGaAs geometry has been investigated. The symmetry broken AlGaAs structure is obtained by roughly removing one quarter of the volume from a nanocylinder, see Figure 2. In the following, we will refer to such design as a 'nano-chair'. The main advantage of using the nano-chair geometry is related to its SH emission properties, specifically, that the dominant component of the nonlinear current presents an even-symmetry distribution consistent with a SH mode having a central lobe emission. Thus, the proposed optimized asymmetric structure successfully breaks the field symmetry inside the dielectric structure. Differently

from an AlGaAs cylinder, which presents a SH null in the forward and backward directions when the pump impinges normally, the optimized nano-chair produces SH nonlinear currents whose symmetry is consistent with a maximum SHG in the normal direction when pumped at normal incidence for the most widely used (100) cylinder axis orientation. Hence, this design can be realized with minimal complexity, in the nanoantenna fabrication and experimental implementation.

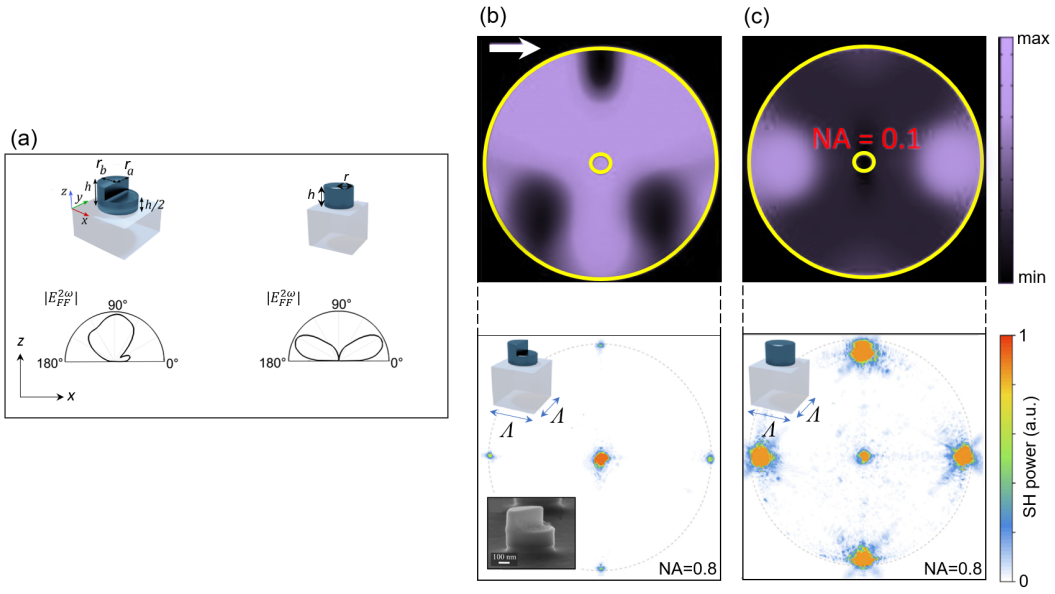

Figure 2: (a) Top: sketch of the nano-chair structure and of the symmetric pillar counterpart. Bottom: the SH far field in the *xz* plane associated with the two unit cells. A plane wave at 1550 nm, *x* polarized, is assumed as the light source. (b) Top: simulated Fourier plane images (*xy* plane) of the SH radiation emitted from an isolated nanochair structure. Bottom: Experimental Fourier-plane images of the SH signal emitted in the forward direction from a uniform array of nanochairs. (c) Same as (b) but for the full nanodisk. The external yellow circle indicates the numerical aperture (NA) equal to 1, while the smallest one indicates NA=0.1. The SHG power has been normalized to its maximum value for a better visualization of all the diffraction orders. Adapted with permission from [67] © The Optical Society.

The nano-chairs ability to radiate the SH along the normal direction makes them attractive as building blocks for nonlinear beam-shaping applications [67]. By considering an AlGaAs element with an elliptical base, one can numerically explore a two-dimensional optimization plane constituted by the two ellipse semi-axis (r_a and r_b). By computing the SH emitted phase and amplitude for each couple, a so-called look-up table (LUT) can be populated. The scope of this table is to highlight the AlGaAs nano-chair geometry that simultaneously guarantee a constant SH field amplitude with a main lobe along the normal direction and a SH phase profile in the far-field which scans the entire range [0,2π) rad. The latter forms the metasurface 'basis', see Figure 3. Once a basis is found, it is used to place the geometrically optimized AlGaAs building blocks in a proper way depending on the phase profile to fulfill. To better elucidate this procedure, in the following we will report two examples: the first is related to SH beam steering, while the second deals with the design of SH metalenses.

In order to guarantee a stable and robust look-up table, [67] reported a smart procedure which consists in first computing the properties of the isolated structures and then minimizing the unit cell size period, Λ, without affecting the far-field emission behavior. For a FW at 1550 nm, the minimum acceptable period is Λ = 900 nm. For smaller periods in fact the collective modes are no longer negligible. Thence, the choice of the periodicity is dictated by a trade-off between the requirement of optically uncoupled nanoantennas and a sub-wavelength sampling necessary to avoid diffraction at the FW. The selected period is slightly larger than the SH wavelength (λ_{SH}=775 nm). Thus, this is inevitably associated with the presence of one diffraction order at large angles. In any case, since the SH radiation pattern of the unitary cell (the AlGaAs nano-chair) is strongly directional along the vertical direction with a single emission lobe close to broadside emission, most of the SH power is radiated to the zero-diffracted order and the first-diffracted order only slightly affects the metasurface performance.

It is interesting to note that the intrinsic nano-chair asymmetry provides an additional degree of freedom regarding the SH phase. Indeed, upon a π rotation of the AlGaAs structure in the *x*,*y* plane, the *z* component of the electric field inside the resonator at FW is π-shifted while the *x* component remains unmodified. Thus, due to the expression of the nonlinear SH polarization in AlGaAs crystalline structure, this implies a π-shift of the *y* component of the emitted SH signal.

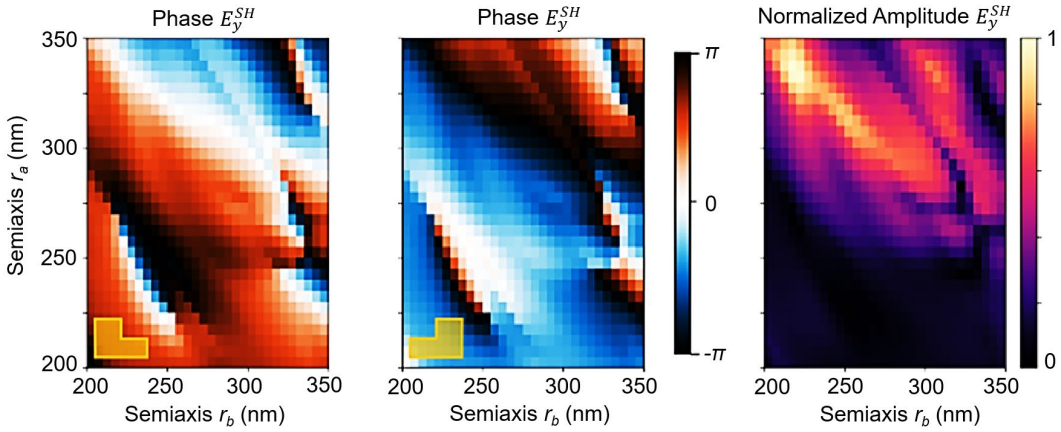

Figure 3: Calculated SHG performance of the nanochair metasurfaces. LUTs of phase and normalized amplitude of the electric far-field y component in the zero-diffracted order in the forward direction. The two phase maps refer to the two orientations of the resonator sketched in the inset. Reprinted with permission from [67] © The Optical Society.

Firstly, let us report the possibility to design, through the usage of the LUT, a nonlinear metasurface implementing a SH beam steering of an angle θ_s. The proposed metasurface is built with a supercell of N=8 nano-resonators. Each of the 8 nano-chairs is designed to implement a sawtooth phase profile that leads to a steering angle $\theta_s=sin^{-1}(\lambda_{SH}/N\Lambda)\approx6.2°$. Figure 4(a) shows the near field SH y-component; this is consistent with the emission of a wavefront with the intended steering angle as experimentally verified in Fig. 4(d) for the fabricated metasurface reported in Fig 4(b). The emission of a uniform nano-chair array is also measured and reported for comparison in Fig. 4(c). This first pilot study demonstrates the beam control capability of this nonlinear metasurface.

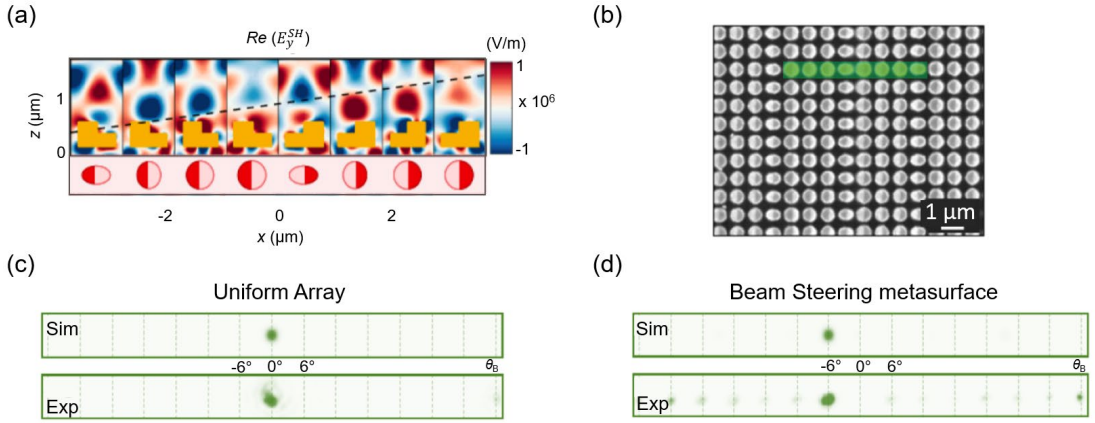

Figure 4: (a): Numerical predicted near field in vicinity of the eight meta-atoms used to steer SH emission. (b): Comparison between the numerical calculations (top) and experimental characterization (bottom) of the far-field SH, for a metasurface designed to steer the SH beam at θ_s=6.2°. (c): SEM image of the fabricated device, with highlighted the eight meta-atom supercell. (d): Comparison between the numerical calculations (top) and experimental characterization (bottom) of the far-field SH, for an array of identical resonators. Reprinted with permission from [67] © The Optical Society.

To elucidate and stress the potential of the 'nano-chair' based approach, we report here the design of nonlinear metalenses. The capability to focus the nonlinear beam into a diffraction-limited spot size represents a new standpoint for nonlinear imaging and microscopy. By imposing an hyperboloidal phase profile, $\varphi_{SH}(x,y)=(2\pi/\lambda_{SH})(\sqrt{f^2+(x^2+y^2)}-|f|)$ for the SH emission, it is possible to focus the SH at a distance f. The design of two lenses with a diameter of 70 μm and focal distances respectively equal to 70 μm and 175 μm has been proven [67]. The geometrical parameters of the resonators are extracted from LUT, by minimizing the difference between the desired phase function $\varphi_{SH}(x,y)$ and the phase emitted by each nano-chair. Concerning the fabrication process, the sample are obtained by a planar structure, grown by molecular beam epitaxy, consisting of a 400 nm- thick $Al_{0.18}Ga_{0.82}As$ layer deposited on a [100] GaAs substrate. A 500 nm- thick $Al_{0.8}Ga_{0.2}As$ sacrificial layer is inserted before the GaAs epitaxial growth. The sample are glued on a sapphire host substrate with a flip-chip process. The growth substrate and the sacrificial layer are then removed by mechanical and selective chemical etching, leaving only the 400 nm -thick GaAs as a mirror-flat surface. Two consecutive e-beam lithography and inductively coupled plasma (ICP) etching processes are needed. A first ICP reactive-ion etching (ICP–RIE) dry etching with $SiCl_4$ transfer the first half of cylinder pattern to the AlGaAs layer for 200 nm thickness, followed

by a second aligned lithography and ICP etching to realize the final nano-chair resonators. The experimental validation of the metasurface performance is done by measuring the SH at different image planes along the propagation axis. The profile of the SH beam, as shown in Fig 5, is obtained by post-processing the collected images. The measured behavior is in good agreement with the theoretical predictions. This realization of nonlinear meta-optics with [0,-2π) rad full phase control is capable to focus the SH beam to a waist, w_0, of $0.84\lambda_{SH}$ with a conversion efficiency that is consistent with real world applications. Table 1 compares the conversion efficiency for relevant studies on nonlinear beam shaping; the impact of the described AlGaAs-based metasurface is highlighted by the comparison of the normalized nonlinear efficiencies with respect to common materials for nonlinear optics such as silicon and gold. Still, the presented performances are mainly limited by the design (only few geometrical parameters are considered) and by fabrication tolerance (size difference between the nominal and fabricated nanostructures). However, in the near future, the design would benefit from implementing machine-learning techniques while the fabrication could exploit pioneering lithographic processes capable of better resolution.

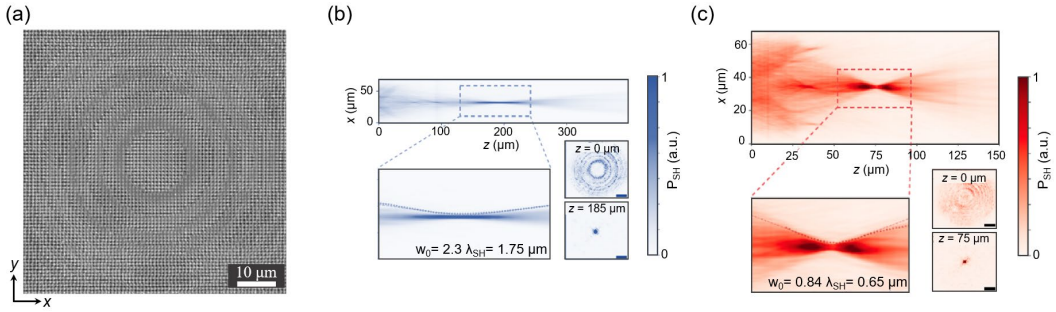

Figure 5. (a) SEM image of a Fresnel lens metasurface designed to focus the SH emitted signal at f=185µm. Nonlinear optical characterization of two Fresnel lenses focusing at (b) f=185 µm and (c) 75 µm, respectively. The magnified region around the focal point reports the beam waist measurement (dots) and the Gaussian beam waist fit (dashed line) used to retrieve the focal spot dimension. The two insets show the SH signal acquired at the metasurface plane and at the focal plane. The scale bars in all four insets are 10 µm long. Reprinted with permission from [67] © The Optical Society.

Reference	Type	NL Efficiency	P_{FF}	I_{FF}	Normalized NL Efficiency
Nat. Mater. 14, 607–612 (2015)	Gold – $\chi^{(3)}$	N/A	1.9 kW	9.3 MW/cm^2	N/A
Nat. Commun. 7, 1–7 (2016)	Gold – $\chi^{(3)}$	$P_{TH}/P_{FF} = 10^{-8}$	6 MW	20 GW/cm^2	$P_{TH}/(P_{FF})^3 = 2.5\ 10^{-22}$ W^{-2}
ACS Photon. 3, 117–123 (2016)	Gold – $\chi^{(2)}$	$P_{SH}/P_{FF} = 10^{-11}$	18 kW	0.22 MW/cm^2	$P_{SH}/(P_{FF})^2 = 6\ 10^{-16}$ W^{-1}
Nano Lett. 18, 3978–3984 (2018)	Silicon – $\chi^{(3)}$	$P_{TH}/P_{FF} = 10^{-6}$	33 kW	N/A	$P_{TH}/(P_{FF})^3 = 9\ 10^{-16}$ W^{-2}
Nano Lett. 20, 4370–4376 (2020)	Silicon – $\chi^{(3)}$	$P_{TH}/P_{FF} = 10^{-6}$	42.3 kW	0.75 GW/cm^2	$P_{TH}/(P_{FF})^3 = 6\ 10^{-16}$ W^{-2}
Nano Lett. 18, 8054–8061 (2018)	Silicon – $\chi^{(3)}$	$P_{TH}/P_{FF} = 10^{-6}$	N/A	33 GW/cm^2	N/A
Optica 8, 269-276 (2021)	AlGaAs – $\chi^{(2)}$	$P_{SH}/P_{FF} = 1.3\ 10^{-5}$	47 kW	0.14 GW/cm^2	$P_{SH}/(P_{FF})^2 = 2.8\ 10^{-10}$ W^{-1}

Table 1: Conversion efficiency for relevant works related to nonlinear beam shaping.

3. Liquid Crystal- based Reconfigurable SHG

In the previous section, the potential of AlGaAs metasurfaces for nonlinear optics has been presented. Thus far, only their static performances were discussed: for a single geometrical design, the metasurface operates at a given incident wavelength and there is no possibility to modulate the nonlinear emission. Recently, the capability to dynamically tune the SH emission has started gaining attention and efforts have been made by several research groups to achieve this goal [78]. A possible reconfigurable implementation of AlGaAs metasurfaces can be obtained through a suitable choice of the metasurface superstrate. i.e. the medium surrounding the meta-atoms. A promising approach is to deposit anisotropic liquid crystal (LC) materials in the metasurface upper region, as shown in Fig. 6 [79]. LCs feature high birefringence in the infrared and thus already find applications in display industries, laser beam steering, tunable crystal fibers and electronic phase shifters [80] [81]. Despite most materials undergo a phase transition from solid to liquid at a melting point, the

peculiarity of LCs is that they exhibit an intermediate phase in which there is some local order due to their molecular shape. Among the several different classes of LCs, nematic ones are the simplest. Nematic LCs can be prototyped as long molecules which tend to align their long molecular axis parallel to their neighbors. The locally averaged molecule direction is indicated as a versor and it is known as the director. Since the molecules are anisotropic, the properties of LCs can be tuned by changing the director. A widely employed nematic LC is the E7-LiMerck, which guarantees an anisotropy of its refractive index almost equal to 0.2 [82] [83]. In particular, if the LC director experiences a planar alignment (i.e. the director is parallel to the x axis, see Fig 6), the non-null elements of the LC refractive index tensor are $n_x=n_e$, $n_y=n_o$, $n_z=n_o$, where n_o and n_e are the refractive indices along the LC ordinary and extraordinary axes. The latter condition is also called unbiased state. Instead, when the LC director is vertically oriented (i.e. toward the z axis, Fig 6b) the homeotropic alignment is considered with $n_x=n_o$, $n_y=n_o$, $n_z=n_e$. Hence, the E7 crystal is a good candidate superstrate of an AlGaAs metasurface for tunable SH generation. Indeed, the LC high birefringence (almost 0.2) will allow the modulation of the linear scattering behavior and thus of the generated SH emission from an AlGaAs-on-AlOx nanodisk metasurface. In the following, we will demonstrate how it is possible to modulate the SH intensity and simultaneously the SH Front-to-Back Ratio (FBR).

Let us consider a metasurface made of AlGaAs nanocylinders on top of an AlOx substrate embedded into a LC matrix, as depicted in Fig 6 [79]. The AlGaAs pillars have radius r = 280 nm and height h = 200 nm. For simplicity, the LC is assumed to switch between the homeotropic and the unbiased state.

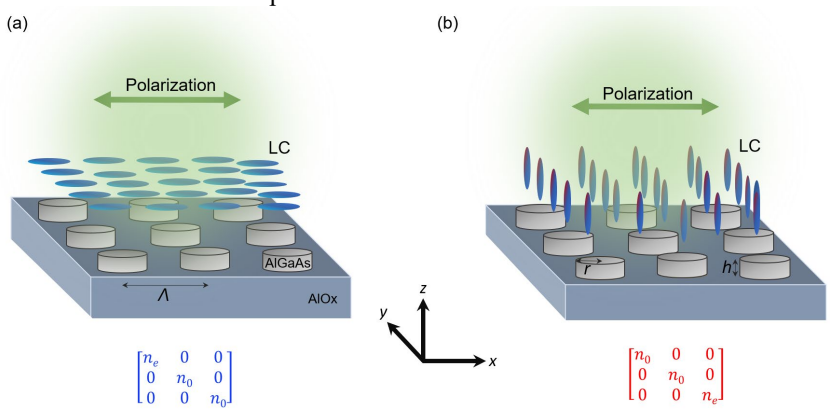

Figure 6. Sketch of the proposed metasurface in the case of LC director (a) parallel to the metasurface (planar alignment) and (b) perpendicular to the metasurface (homeotropic alignment). The green arrow represents the fixed incident light polarization. Adapted with permission from [79] © The Optical Society.

The period Λ is set to 909 nm. The geometrical parameters of the metasurface are optimized to maximize the variation of the SH emission upon a full reorientation of the LC director. The excitation is assumed to be a plane wave of wavelength 1550 nm perpendicularly incident on the metasurface with a fixed polarization of the electric field along the x axis. All the numerical predictions are obtained with Finite Element Method simulations in Comsol Multiphysics. In order to take into account dispersion, the anisotropic refractive index of the LC is defined with n_e=1.7030 and n_o=1.5020 for the fundamental wavelength and n_e=1.7209, n_o=1.5120 for the SH frequencies [79]. These values are in agreement with what already reported for E7 LC at a working temperature of 20 °C. Figure 7 shows the linear transmittance for the two considered LC states. As expected, the change in the refractive index above the metasurface translates into a sizable modification of the scattering emission from the nanodisks. In particular, the multipolar decompositions in Figure 7b and c reveals that the electric dipolar (ED) resonance is excited at 1496 nm and around 1630 nm for the planarly oriented LC and at 1550 nm in the homeotropic LC alignment. On the other hand, the magnetic dipolar (MD) resonance red shifts from 1508 nm to 1580 nm after a complete re-alignment of the LC director.

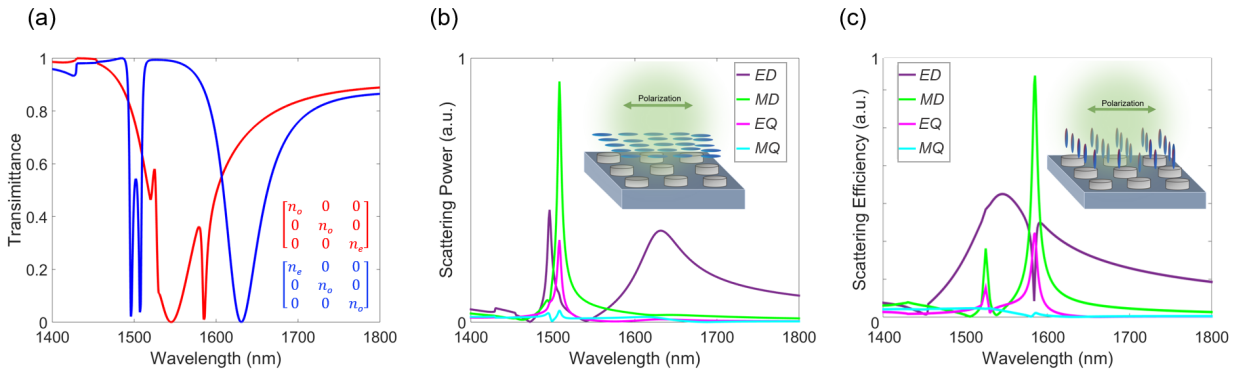

Figure 7. (a) Simulated transmittance of the metasurface for the two LC orientations: the blue (red) curve refers to the LC directors parallel to the *x* (*z*) axis. multipolar scattering decomposition for LC directors oriented parallel (b) or orthogonal (c) to the *x* axis. The coefficients *ED, MD, EQ* and *MQ* are associated to electric dipole, magnetic dipole, electric quadrupole, and magnetic quadrupole contributions, respectively. Adapted with permission from [79] © The Optical Society.

The SH predictions are also performed by Comsol Multiphysics by introducing the SH sources in terms of current densities determined by the field distribution at the pump frequency. Moreover, the zincblende [100] crystallographic direction is assumed aligned to the *x* Cartesian axes. In the model, only AlGaAs is assumed as a nonlinear medium because both the substrate and the LC have negligible second-order susceptibility. Figure 8 reports the total SH efficiency, that is the ratio between the total scattered SH power and the incident power on the unitary cell area, for the two considered director orientations. The SHG peaks are associated to the excitation of the MD resonance at the fundamental wavelength. The maximum SHG is reached at 1508 nm for the LC planar orientation and around 1580 nm for the homeotropic case. Please note, that for a fixed wavelength, a SH modulator is obtained thanks to the possibility to excite or not a magnetic dipolar resonance when switching the LC state. However, as previously anticipated, the absolute value of the efficiency is not the only relevant quantity. Experimentally one can detect only over a finite solid angle, typically in a transmission or backscattering geometry. It is therefore important to characterize the directionality of the emission and optimize it according to the specific experiment needs. In reflection set-up geometries it is fundamental to know how much of the generated SH is emitted towards the upper region. In this case, the quantity to maximize is the SH Front-to-Back Ratio (FBR), that is defined as the ratio between the SH power emitted in the LC region by the SH power scattered in the substrate. Figure 8b reports the obtained SH FBR for the considered LC orientations. Note that, at a pump wavelength of 1580 nm (the wavelength for which a magnetic dipolar resonance is excited at the fundamental) for the LC oriented in the homeotropic alignment, the FBR peaks at about 6.5. Correspondingly, at the same wavelength, the FBR for the other LC state is 0.65. This achievement highlights the capability of the presented meta-structure to modulate also the SH FBR by the LC alignment. Importantly, for a fixed wavelength excitation, an enhancement of one order of magnitude in the nonlinear FBR is reached. Figure 8c further elucidates the different SH field distributions at the peak of nonlinear emission efficiency for the two considered LC orientations. Figure 9 presents the plot of the field inside the nanodisk at the resonances for the two LC orientations. The plot of the SH emission variation upon full re-orientation of the LC director is also reported as a function of the geometrical parameters.

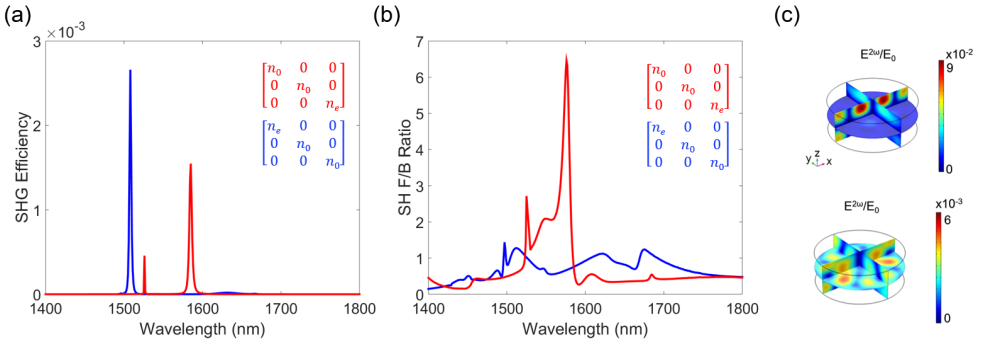

Figure 8. (a) Second- harmonic efficiency as a function of the fundamental wavelength for LCs in a planar alignment (director parallel to the *x* axis, blue curve) and in a homeotropic one (director oriented along the *z* axis, red curve). (b) Numerical calculations of the second harmonic FBR as a function of the fundamental wavelength for the two LC orientations. (c) Second- harmonic field distribution inside an AlGaAs cylinder of the metasurface (top) for an incident wavelength of 1497 nm for the LC director oriented in the *xy* plane and (bottom) for an excitation wavelength of 1576 nm and LC aligned in the *xz* plane. The plots are normalized to the incident electric field E_0. Adapted with permission from [79] © The Optical Society.

To conclude, in this section, we have exemplified the possibility to obtain a nonlinear SH modulator by using LCs as the superstrate of a dielectric metasurface. By switching between two LC states (planar or homeotropic), the SH signal can be switched on or off. In addition, the LC anisotropy allows to modulate the FBR ratio of the emitted SH. These presented numerical predictions represent a preliminary study for the implementation of dynamically tunable mateasurfaces, which might have various applications, including active beam shaping and tunable imaging.

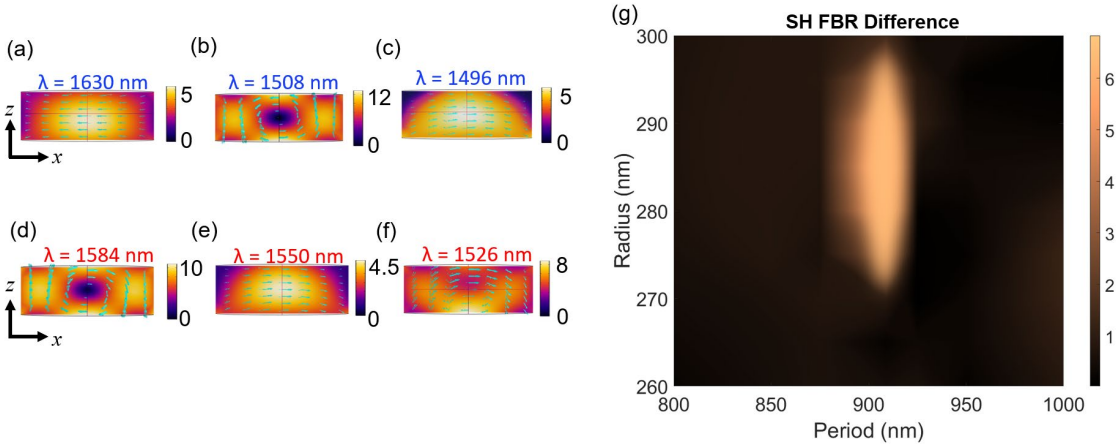

Figure 9. (a), (b) and (c) show the electric field distribution map inside the dielectric nanodisk for a planar LC alignment and an incident wavelength equal to 1630 nm, 1508 nm and 1496 respectively. The electric field enhancement inside the resonator for the homeotropic LC orientation is plotted in (d), (e) and (f) for wavelengths equal to 1584 nm, 1550 nm and 1526 nm, respectively. The green arrows refer to the electric field vector. (g) SH Front-to-Back Ratio Difference for the two different LC orientations as a function of the radius of the AlGaAs nanodisks and the period of the metasurface. The incident signal is assumed to be a *x*-polarized plane wave at 1576 nm wavelength. The height of the pillar is fixed to 200 nm. Adapted with permission from [79] © The Optical Society.

4. Thermo-optical SHG modulation

As stated above, all-optical reconfigurability in the nonlinear regime is attracting today a great deal of interest for basic science and applications [84] [85] [86]. In the previous section, the perturbation of the surrounding material by means of an anisotropic medium has been extensively discussed as an approach to modulate the SH power. Very recently, the use of an optical external stimulus (which is responsible for increasing the temperature of dielectric nanodisks) has been reported as the control modulating the nonlinear signal [87]. Indeed, by increasing the temperature of the nanoresonators, it is possible to modulate their emitted SH light. Here, we report two approaches: the heating can be thermally provided by utilizing a Peltier cell or it can be optically supplied by a Continuous Wave (CW) optical excitation above the nanoantenna bandgap. We define the modulation of the SH as: $\Delta_{SHG}=(I_{SHG}^{ON}-I_{SHG}^{OFF})/I_{SHG}^{OFF}$ where I_{SHG}^{ON} is the SH intensity emitted by the resonator in presence of the heating stimulus (i.e. when the samples are heated by the Peltier cell or with the CW pump excitation) and I_{SHG}^{OFF} stems for SH intensity emitted by the unperturbed AlGaAs cylinders. Thus, I_{SHG}^{ON} is a function either of the temperature imposed by the Peltier cell or of the power of the control CW signal. The sample that was investigated is made of AlGaAs-on-AlOx nanodisks 3 μm apart from each other with the same height (equal to 400 nm) and with different radii in the range between 195 nm and 215 nm. The sample is grown by molecular beam epitaxy on a [100] GaAs wafer, with 400 nm layer of $Al_{0.18}Ga_{0.82}As$ on top of an $Al_{0.98}Ga_{0.02}As$ substrate to be oxidized at later stage. An electron-beam lithography process is then applied to obtain an array of nanodisks. The expected tunable behavior can be experimentally tested with a non-linear confocal microscope, as depicted in Fig. 10. The pump light is delivered by a linearly polarized ultrafast (160 fs pulse duration) erbium-ytterbium-doped laser at 1550 nm and it is focused to a diffraction-limted spot size of 1.8 μm onto the sample by a high-numerical aperture (NA=0.85) air objective. The experimentally detected SHG from pillars with different radii is presented in the inset of Fig. 10d for a pulse with a peak intensity equal to 1 GW/cm^2.

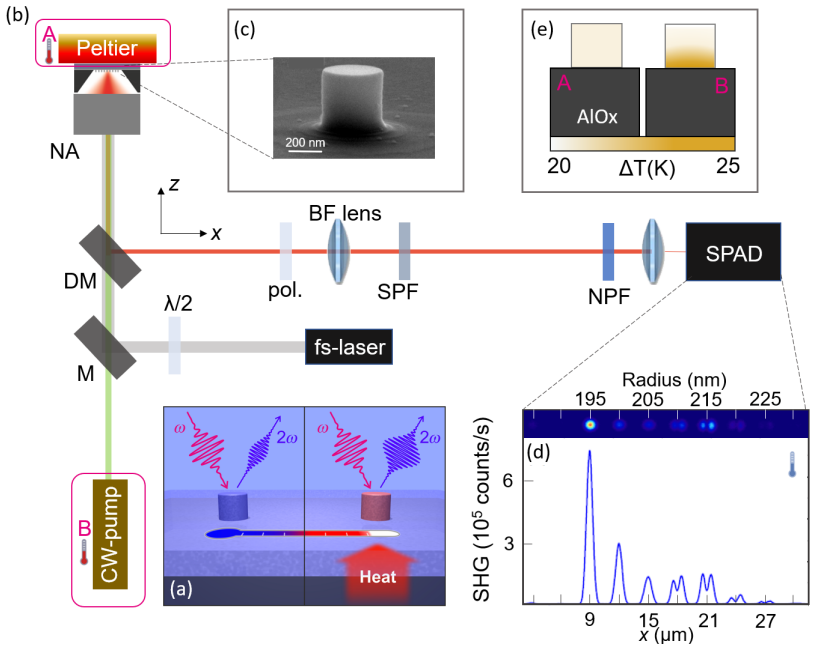

Figure 10. (a) Sketch of the tuning mechanism of the SH signal through a heating source. (b) Experimental setup used for the optical measurement for the case of Peltier cell or CW-pump control signal. (c) Scanning electron microscopy image of an AlGaAs nanoresonator. (d) Measured SH signal in unperturbed conditions as a function of the pillar radius. (e) Theoretical predictions of the temperature distribution for the nanodisk excited with the Peltier cell (left) or with the CW-pump (right). Adapted with permission from [87] © The Optical Society.

Firstly, we report the results obtained in the case of Peltier cell heating. In this case, the nanodisk is heated by conduction . Indeed, the sample substrate adheres to the Peltier cell which imposes, at equilibrium, a constant temperature equal to $T_0+\Delta T$, being T_0 the room temperature. The high thermal conductivity of the nanodisk results in a nearly uniform temperature inside it , almost equal to $T_0+\Delta T$. This assumption is corroborated by numerical predictions in Comsol Multiphysics. In the numerical model, the substrate is decomposed in three elements: the AlOx layer closer to the nanoresonator, the GaAs central layer, and a layer that mimics the presence of a highly conductive carbon tape inserted between the substrate and the Peltier cell in order to guarantee a good thermal contact. The AlGaAs, AlOx and GaAs thermal conductivity are selected in agreement with previous references [88] [89]. Instead, the thermal conductivity of the carbon tape is experimentally estimated as 100 W/(m K) [87]. Moreover, at the interface between the AlGaAs nanodisk and the AlOx sublayer a thermal boundary conductance of 10 MW/(m^{2}K) is assumed. Fig. 10(e) reports the results of the thermal simulations: the temperature differs by less than 0.05 K with respect to the one set on the Peltier cell. Thus, the temperature distribution inside the AlGaAs structure can be considered uniform and equal to $T_0+\Delta T$. Fig. 11a shows the differential SH signal measured on five nominally identical particles when $\Delta T = 20$ K. to estimate the relative SHG intensity variation, the SHG maps under unperturbed conditions are subtracted from the ones measured by varying the temperature. Next, the SHG modulations maps are normalized by the map measured without any heating mechanism. During this normalization process, a threshold needs to be set to the background level, otherwise extremely low counts would lead to saturated pixels in the SHG modulation maps. Ultimately, to prevent small errors and assign an unambiguous value at the modulation, the signal obtained is integrated around each individual resonator. Fig. 11b summarizes the obtained nonlinear modulation when ΔT=10 K and ΔT=20 K: a moderately small temperature increase of 20 K is associated with a sizable SH modulation of roughly 20%. To gain further insight into this result, a thermo-optical modeling is proposed. In doing so, the thermal change of the AlGaAs refractive index, n, is calculated as $\Delta n(T,\lambda)=(dn/dT)\,\Delta T$ [90] [91]. The trend of dn/dT is reported in Fig. 11c: it is about 10^{-4} K^{-1} around 1550 nm and rapidly increases as the wavelength approaches the one corresponding to the band edge. Hence, designing Mie resonances for efficient SHG around the band edge is a crucial aspect for boosting the thermal nonlinear modulation. The proposed thermo-optical model is then employed to calculate the SHG modulation due to the thermally induced refractive index variations via finite element simulations in Comsol Multiphysics. Fig 11d reports the calculated results, which are in good agreement with the experimental ones. Small discrepancies are attributed to fabrication uncertainty on the nominal radius of the AlGaAs pillars.

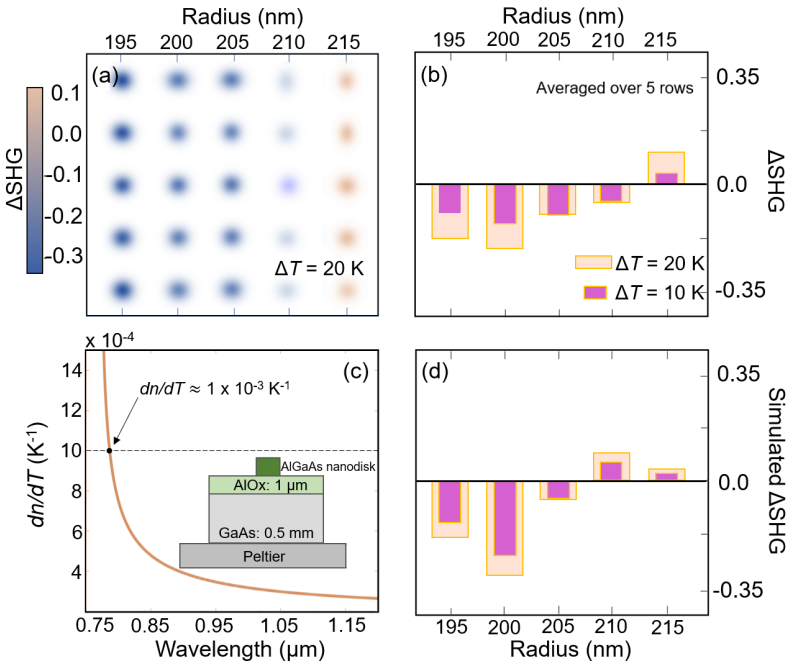

Figure 11. (a) ΔSHG(T_0 + 20 K) measured on five replicas (from top to bottom) of five nanopillars of increasing radius. The average of $\Delta SHG(T_0 + \Delta T)$ over each column in panel (a) is reported as magenta and orange histograms in panel (b), for the five different radii and two different temperatures (ΔT = 10 K and ΔT = 20 K). (c) Theoretical model of *dn/dT* versus wavelength. Inset: schematic of the Peltier cell heating. (d) Modeling data to be compared with the experimental data reported in panel (b). Adapted with permission from [87] © The Optical Society.

Secondly, we describe the case where heating is achieved by means of an optical control signal with specific incident power, P_p. Although the Peltier cell heating procedure allows us to reach sizable modulation even for small temperature increase, all-optical control is a more attractive approach since it allows to selective heating of the individual nanoobjects (eventually the heating of only one single metaatom within a metasurface). The latter approach consists of using an auxiliary CW pump beam with photon energy well above the AlGaAs band gap as the control. The beam is tightly focused on the nanodisk with a spot size of 1 μm at a wavelength of 405 nm (well above the AlGaAs band gap). The measured SH modulation is reported in Fig. 12a. One can notice that the two heating mechanisms lead to similar results. The main difference between the two approaches is related to the temperature gradients within the AlGaAs nanodisk. Indeed, the effects of the CW signal has been also modeled with opto-thermal simulations. In this scenario, the control CW light is absorbed by the resonator inducing an increase of the temperature. Our numerical calculations show a non-homogeneous electric field distribution inside the nanodisk, corresponding to a strong light absorption at the top surface of the dielectric cylinder. Therefore, contrarily to the Peltier cell heating, in the all-optical approach the non-uniform optical absorption yields a non-uniform thermal heating, which finally translates in a non-uniform refractive index. This is the reason why different amplitude SH modulations are observed with respect the Peltier cell heating.

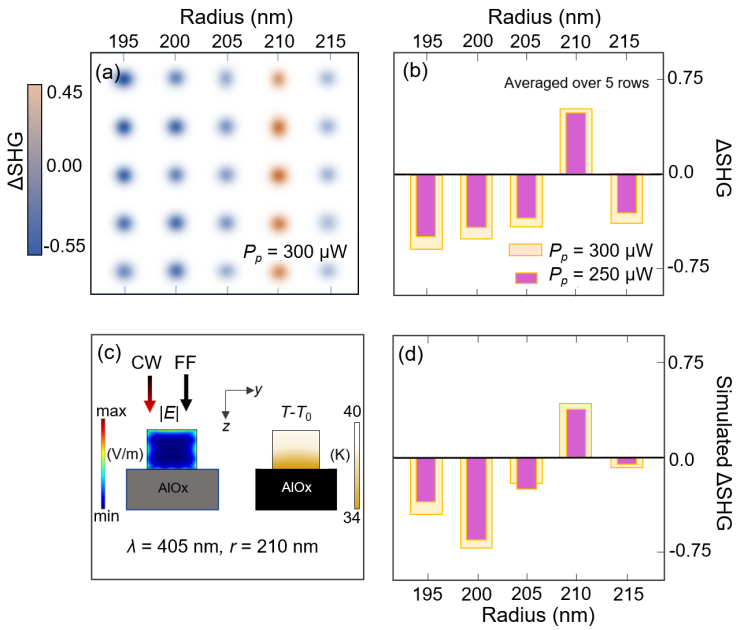

Figure 12. (a) Measured differential SH signal (ΔSHG(*P*p)) collected by scanning five replicas of nanopillars of increasing radius with a control beam power *Pp* = 300 μW and wavelength of 405 nm. (b) ΔSHG(*Pp*) for five different NP radii for two control pump powers (*Pp* = 250 μW and *Pp* = 300 μW). (c) Schematic of the optical heating (left) and induced temperature field in the NP (right) for Pp = 300 μW. (d) Modeling data to be compared with the experimental data in panel (b). Adapted with permission from [87] © The Optical Society.

The all-optical heating approach has been studied as a function of the CW control power and for two CW wavelengths, i.e. 405 nm and 532 nm. Figure 13 summarizes the obtained results. In more detail, the nonlinear modulation can be tuned by the CW input by up to 60%. Interestingly, even if the AlGaAs absorption coefficient decreases with the wavelength, the SHG modulation is almost the same for the two CW pumps. This counterintuitive phenomenon is explained by Fig. 13, where the absorbed power density in the same nanoresonator for the two CW wavelengths is reported for a fixed *Pp*. It is clear there that the excitation at 532 nm undergoes the stronger absorption due to the excitation of higher-order Mie resonances.

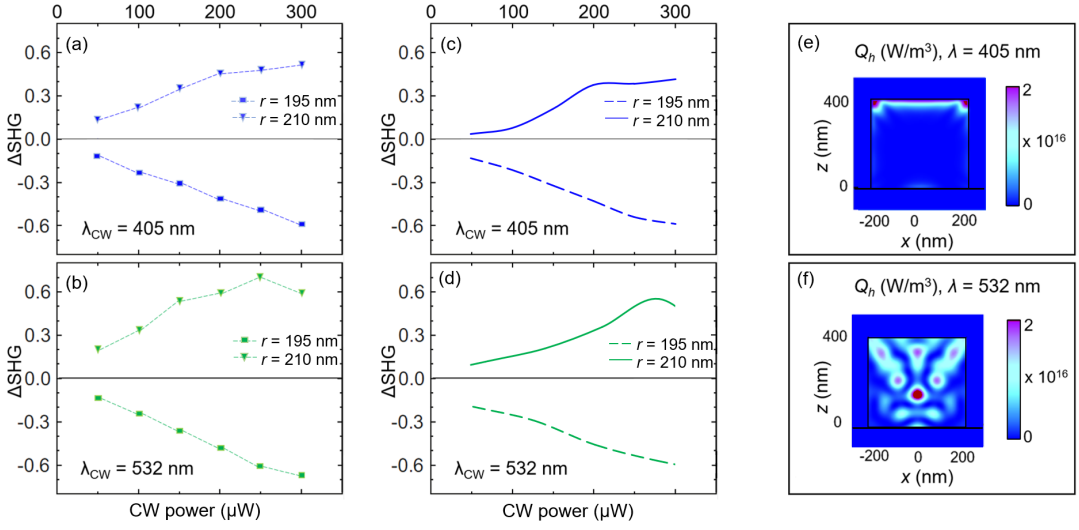

Figure 13. (a), (b) Measured and (c), (d) simulated SHG modulation for two pillar radii versus control beam power for a control wavelength of (a), (c) 405 nm and (b), (d) 532 nm. Absorbed power density for a nanoresonator with radius 210 nm, excited with a control beam with power *Pp* = 300 μW and wavelength (e) 405 nm or (f) 532 nm. In panels (a)–(d), a positive (negative) modulation corresponds to a pillar radius of 210 nm (195 nm). Adapted with permission from [87] © The Optical Society.

Regarding the switching speed of the proposed nonlinear modulator, there are two aspects to consider: the time necessary to reach the steady-state temperature after the pump is turned on and the time necessary to recover the initial

room temperature once the control signal is switched off. Numerical predictions indicate that the heating and the cooling processes are both completed after about 100 ns. To draw this conclusion, time-dependent simulations in Comsol Multiphysics have been performed; a control CW signal (wavelength of 405 nm) with intensity equal to 200 kW/cm^2 is used to excite the nanodisk. Under steady-state illumination, the nanodisk's spatially- averaged temperature exceeds the room temperature (T_0) by 58 K. To model the heating process, it is assumed that the nanodisk is initially (at time t=0) cold (i.e. at room temperature) and the light is turned on at the time $t_0 \approx 10^{-13}$ s. The steady-state temperature is reached after 100 ns (as shown in Fig. 14, purple curve). The cooling process is modeled starting from a steady-state initial condition, where the nanodisk is illuminated with the CW wave and the nanodisk is hot (ΔT=58K). The CW pump is turned off at the time $t_0 = 10^{-13}$ s. Again, the simulations predict that the time to cool down anto the room temperature is about 100 ns (Fig. 14, green curve). Thus, the external thermal tuning can be translated into a dynamical tailoring of the SH emission with a modulation frequency up to 10 MHz.

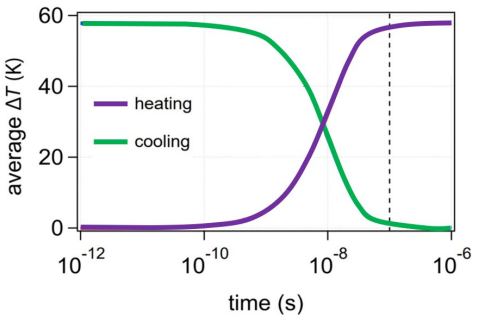

Figure 14. Average nanodisk's temperature ΔT vs time for a nanodisk with r = 200 nm and height equal to 400 nm, for heating (purple curve) and cooling (green curve) processes. The heating is due to a CW signal at a wavelength of 405 nm and with intensity equal to 200 KW/cm^2. The black dashed vertical line highlights the time 100 ns, at which the steady state is reached. Adapted with permission from [87] © The Optical Society.

To conclude, in this section, the thermo-optical modulation of the SH emitted signal was presented. In particular, we have reported that by using a strongly absorbed control beam that impinges on a nanodisk, all-optical control of SHG is possible in AlGaAs-on-AlOx platform. A SHG modulation up to 60% is numerically and experimentally reached for a modest temperature increase of about 40 K. This large modulation in an isolated meta-atom represents a promising result for obtaining all-optically tunable nonlinear metasurfaces whose meta-atoms can be addressed individually.

5. Perspectives

The discussion presented so far has focused on the tunability of the nonlinear effects at the nanoscale coming from dielectric platforms. However, a crucial aspect to be pursued is the harmonic generation efficiency, and in particular the increase of the latter. As aforementioned stated in Sections 1 and 2, several approaches have been proposed [92, 93, 94]. Among all the possible solutions, let us underline here the huge potential of hyperbolic metamaterials, epsilon-near-zero media and nonlinear metasurfaces based on bound-states in the continuum. The use of these mechanisms – and a combination of them – can push the generation of harmonic frequencies towards extremely efficient regimes.

In more details, implementations of hyperbolic metamaterials are obtainable as alternating layers of dielectrics and metals [95], acting like a dielectric in the direction orthogonal and as a metal in the direction parallel to the interfaces, or as wire media [96] or plasma wires [97] in a dielectric background, which behave like a metal in the direction of the wires axes and like a dielectric in the directional orthogonal to them. Please note that in order to mimic uniform media, the transverse dimensions of the structural elements must be much smaller than the radiation wavelength. Several efficient nonlinear effects in hyperbolic metadevices have been proposed with specific focus on all-optical modulation, non-local enhancement, power-dependent transmission and polarization switching [98, 99, 100, 101, 102].

Another valuable approach for enhancing nonlinear effects is given by epsilon-near-zero (ENZ) platforms. ENZ materials have gained lots of attention due to their specific linear properties [103, 104]. The ENZ condition occurs when the real part of the dielectric permittivity crosses the zero and it may be found in natural (e.g., some noble metals, several semiconductors and various polar dielectrics) or artificial materials (metamaterials). The latter are more adjustable both in terms of absorption losses and zero-crossing wavelength [105, 106]. The capability of the ENZ material to realize perfect electromagnetic tunneling and to re-direct antennas electromagnetic radiation have made them extremely promising in several research fields [107, 108, 109]. In particular, it has been reported that when an antenna is layered on top of an extremely low-permittivity substrate, the air represents the "denser" substance with higher relative permittivity and hence the antenna pattern is mostly emitted into the air region. Moreover, ENZ materials are excellent platforms for nonlinear

processes and especially for harmonic generation [110, 111, 112]. In this context, ENZ substrates can boost harmonic generation processes when the ENZ mode is associated with localized surface plasmon resonances in the case of metallic nanoelements [113, 114]. Similarly, it has been recently proved that the intrinsic ability of ENZ substrates to re-direct the electromagnetic radiation can seriously increase the efficiency of nonlinear processes emitted in dielectric nanoantennas [115]. More specifically, it has been demonstrated that the presence of the ENZ substrate can enhance the emitted SH signal from an isolated cylindrical AlGaAs nanoantenna up to three orders of magnitude with respect to a dielectric substrate and up to two orders of magnitude with respect to a metallic one. This conspicuous improvement has been achieved by exploiting concurrently the high electric field enhancement induced inside the resonator at the fundamental wavelength and the ENZ condition at the SH wavelength, see Figure 15. It has also been demonstrated that the losses in the ENZ substrate are directly responsible for the ability to re-direct the radiation at the harmonic frequency: the huge enhancement in the emitted nonlinear signal comes in truth from the synergy of low losses and the ability of the substrate to behave as a good reflector [116].

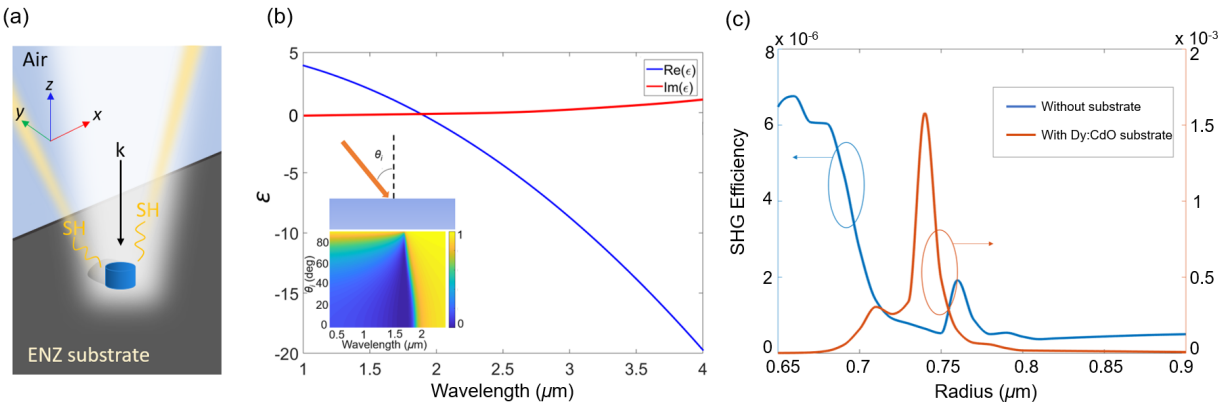

Figure 15. (a) Sketch of the proposed AlGaAs nanoantenna layered over an ENZ substrate, namely Dy:CdO. The optimized cylindrical antenna has a radius of 0.74 μm and a height of 1 μm. Adapted with permission from [115]. (b) Real and imaginary part of the dielectric permittivity of the Dy:CdO substrate as a function of wavelength. The inset reports the reflectance in the case of air/Dy:CdO interface for different incident angles as a function of the excitation wavelength. (c) The SHG efficiency of the AlGaAs nanodisk with height of 1 μm and radius between 0.65 and 0.9 μm in the case of homogeneous surrounding medium, blue line (assumed to be air in the simulation), and in the case of Dy:CdO substrate, orange line. Adapted with permission from [116] https://doi.org/10.1016/j.optcom.2019.124570.

Lastly, let us recall here the concept of BIC-based nanoplatforms. The BIC originates from the complete destructive interference of two or more waves, effectively suppressing all radiative losses [74] [117, 118]. This condition to be satisfied would require infinitely extended devices or materials with either infinite or zero permittivity. However, dielectric nanoparticles support leaky modes which can be geometrically calibrated. Leaky modes with comparable far-field distributions can eventually experience a strong coupling regime featuring avoided resonance crossing. This translates in one of the two leaky modes displaying an extraordinarily high Q-factor for isolated nanoparticles. Such a circumstance is named accidental BIC or quasi-BIC and is of paramount importance for harmonic generation. Indeed, the quasi-BIC exhibits exceptionally high conversion efficiency for SHG and THG in dielectric nanoresonators [119, 120]. More recently, it has been presented an efficient way to realize multifrequency and cascaded parametric nonlinear processes at the nanoscale by combining modes of dielectric nanoresonators originating from the BIC concept with a nontrivial engineering of the substrate [121]. In particular, the engineered multilayered substrate is made of a layer of epsilon-near-zero (ENZ) material sandwiched between a thin layer of an insulator and a dielectric substrate. The substrate undergoes a transition from an insulator to a conductor via an epsilon-near-zero (ENZ) regime. By combining the properties offered by the quasi-BIC mode and ENZ substrate, it has been demonstrated a boost of the efficiency of nonlinear effects at the nanoscale at least by two orders of magnitude in comparison with wavelengths detuned from the quasi-BIC, see Figure 16 [121].

These results imply that the most complete procedure to enhance nonlinear processes from nanodevices should be based on the designing of the whole photonic system instead on the mere engineering of the unloaded and individual nanoresonator.

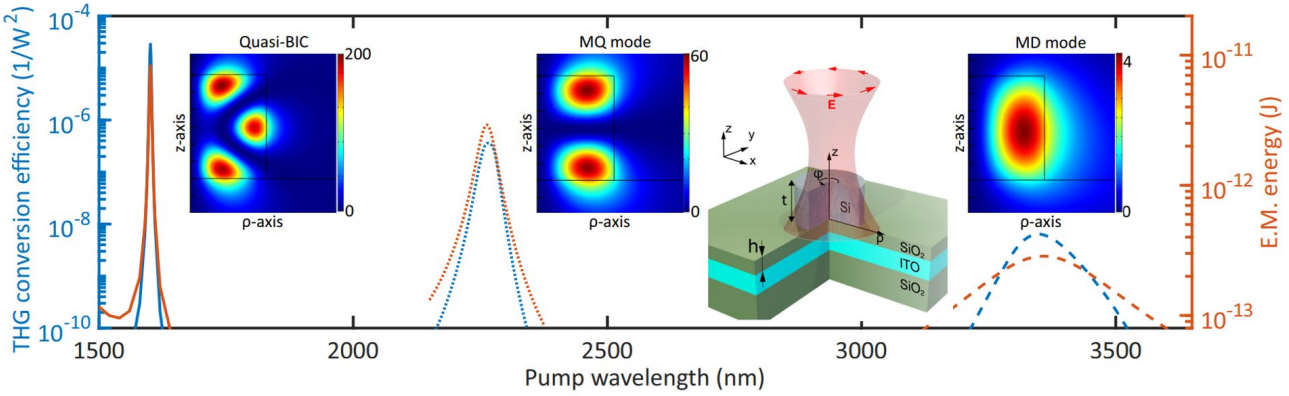

Figure 16. Conversion efficiency for THG as a function of the pump wavelength close to quasi-BIC, magnetic quadrupole (MQ) mode, and magnetic dipole (MD) mode. Electromagnetic energy in the disk at the pump wavelength is shown on the right *y* axis. The three panels show the electric field enhancement in the (ρ, z) plane at an incident wavelength of 1601 nm (quasi-BIC), 2260 nm (MQ mode), and 3360 nm (MD mode), respectively. The pictorial sketch displays the whole structure: the Si disk resonator is placed on top of a multilayer substrate. This is composed of a SiO_2 layer of thickness h, a 300-nm layer of ITO, and another semi-infinite layer of SiO_2. Adapted with permission from [121] https://doi.org/10.1103/PhysRevResearch.1.023016.

6. Conclusions

Metamaterials and metasurfaces have led to the realization of novel electromagnetic properties and functionalities through tailoring subwavelength structures and integrating functional materials. In this chapter, the recent achievements in nonlinear dielectric metasurfaces have been reviewed, with a focus on reconfigurable harmonic generation. In particular, the discussion analyzed the cases of metasurfaces composed of AlGaAs nanodisks. Firstly, the attention is given to the use of LCs which represent an interesting perspective for obtaining nonlinear tunable metasurface. We have reported a device where the dielectric metasurface is embedded in a LC material. We reported the modulation of SH signal in terms of emitted nonlinear power and directionality by predicting a 10-fold enhancement in the Front-to-Back ratio of the SH signal for a fixed incident wavelength for two different LC states. Secondly, the possibility to tune the SH signal by an external source is presented. Using a strongly absorbed control beam that excites a nanoresonator, we have discussed all-optical control of SHG in AlGaAs nanoresonators. The opto-thermally induced perturbation of the refractive index of the nanoantenna is utilized to modify the amplitude of the emitted SH light. Modulation of the efficiency up to 60% is experimentally reached for a modest temperature increase of about 40 K.

Numerical simulations exhibit promising capability of reproducing such features with high fidelity. This is an asset of crucial relevance for designing nonlinear metasurfaces featuring dynamic accurate control of the harmonic generated photons. Currently, the modulation of the second-order nonlinear effects is focused on the amplitude variations of the emitted nonlinear signal [122]. However, this is just the preliminary step toward the investigation of other interesting dynamic variations, such as for example, the phase of the harmonic emitted light. The dynamic phase control of the nonlinear harmonic signal could be used to achieve reconfigurable nonlinear metasurfaces with applications as metalenses or for tunable nonlinear beam steering. Hence, if accurately mingled with the high nonlinear conversion efficiency, dielectric metasurfaces would provide a powerful tool for designing new generations of on-chip nonlinear devices with boosted capabilities based on high-quality optical resonances. It is evident that there are exciting promises for nonlinear nanophotonic metasurfaces that need to be investigated in the near future. For instance, several nonlinear optical functions could be combined on a single ultrathin photonic device.

To conclude, we foretell that upcoming innovation will request a weighty increase in photonic integration and energy efficiency far beyond those of bulky traditional optical instruments. The latter progress can be reached solely by embedding the photonic features at the medium stage, designing a new prototype of metadevices. Reconfigurable photonic metasurfaces will reveal innumerable new pioneering functionalities, possibly being capable to cover even broader applications. Enhancement and improvement of harmonic generation by metasurfaces will further boost the efficiency of frequency mixing used in frequency down- and up-conversion processes together with novel strategies for all-optical tunable control of light waves at the the nanoscale.

Acknowledgement

We thank Giuseppe Marino, Francesco Rusconi, Andrea Mazzanti, Lavinia Ghirardini, Eva Pogna, Camilla Baratto, Paolo Biagioni, Lamberto Duò and Giulio Cerullo for useful discussion.

Funding

European Commission Horizon 2020 H2020-FETOPEN2018-2020 (899673); National Research Council, Joint Laboratories program (SAC.AD002.026); Italian Ministry of University and Research (2017MP7F8F).

References

[1] G. Della Valle, B. Hopkins, L. Ganzer, T. Stoll, M. Rahmani, S. Longhi, Y. S. Kivshar, C. De Angelis, D. N. Neshev and G. Cerullo, «Nonlinear Anisotropic Dielectric Metasurfaces for Ultrafast Nanophotonics,» *ACS Photonics,* p. 2129–2136, 2017.

[2] Y. Yang, W. Wang, A. Boulesbaa, I. I. Kravchenko, D. P. Briggs, A. Puretzky, D. Geohegan and J. Valentine, «Nonlinear Fano-Resonant Dielectric Metasurfaces,» *Nano Letters,* pp. 7388-7393, 2015.

[3] Y. Gao, Y. Fan, Y. Wang, W. Yang, Q. Song and S. Xiao, «Nonlinear Holographic All-Dielectric Metasurfaces,» *Nano Letters,* pp. 8054-8061, 2018.

[4] G. Grinblat, Y. Li, M. P. Nielsen, R. F. Oulton and S. A. Maier, «Efficient Third Harmonic Generation and Nonlinear Subwavelength Imaging at a Higher-Order Anapole Mode in a Single Germanium Nanodisk,» *ACS Nano,* pp. 953-960, 2016.

[5] Z. Zhang, D. Wen, C. Zhang, M. Chen, W. Wang, S. Chen and X. Chen, «Multifunctional Light Sword Metasurface Lens,» *ACS Photonics,* p. 1794–1799, 2018.

[6] N. Yu and F. Capasso, «Flat optics with designer metasurfaces,» *Nature Materials,* vol. 13, pp. 139-150, 2014.

[7] M. Khorasaninejad, W. T. Chen, R. C. Devlin, J. Oh, A. Y. Zhu and F. Capasso, «Metalenses at visible wavelengths: Diffraction-limited focusing and subwavelength resolution imaging,» *Science,* vol. 352, n. 6290, pp. 1190-1194, 2016.

[8] T. Shibanuma, G. Grinblat, P. Albella and S. A. Maier, «Efficient Third Harmonic Generation from Metal–Dielectric Hybrid Nanoantennas,» *Nano Letters,* pp. 2647-2651, 2017.

[9] K. Koshelev, S. Kruk, E. Melik-Gaykazyan, J.-H. Choi, A. Bogdanov, H.-G. Park and Y. Kivshar, «Subwavelength dielectric resonators for nonlinear nanophotonics,» *Science,* pp. 288-292, 2020.

[10] R. Camacho-Morales, M. Rahmani, S. Kruk, L. Wang, L. Xu, D. A. Smirnova, A. S. Solntsev, A. Miroshnichenko, H. H. Tan, F. Karouta, S. Naureen, K. Vora, L. Carletti, C. De Angelis and Jagadish, C. «Nonlinear Generation of Vector Beams From AlGaAs Nanoantennas,» *Nano Letters,* pp. 7191-7197, 2016.

[11] M. Kauranen and A. V. Zayats, «Nonlinear plasmonics,» *Nature Photonics,* pp. 737-748, 2012.

[12] G. Li, S. Chen, N. Pholchai, B. Reineke, P. W. H. Wong, E. Y. B. Pun, K. W. Cheah, T. Zentgraf and S. Zhang, «Continuous control of the nonlinearity phase for harmonic generations,» *Nature Materials,* vol. 14, pp. 607-612, 2015.

[13] E. Almeida, O. Bitton and Y. Prior, «Nonlinear metamaterials for holography,» *Nature Communications,* vol. 7, pp. 1-7, 2016.

[14] S. Keren-Zur, O. Avayu, L. Michaeli and T. Ellenbogen, «Nonlinear Beam Shaping with Plasmonic Metasurfaces,» *ACS Photonics,* vol. 3, pp. 117-123, 2016.

[15] P. Albella, R. Alcaraz de la Osa, F. Moreno and S. A. Maier, «Electric and Magnetic Field Enhancement with Ultralow Heat Radiation Dielectric Nanoantennas: Considerations for Surface-Enhanced Spectroscopies,» *ACS Photonics,* pp. 524-529, 2014.

[16] M. Celebrano, X. Wu, M. Basselli, S. Großmann, P. Biagioni, A. Locatelli, C. De Angelis, G. Cerullo, R. Osellame, B. Hecht, L. Duò, F. Ciccacci and M. Finazzi, «Mode matching in multiresonant plasmonic nanoantennas for enhanced second harmonic generation,» *Nature Nanotechnology,* pp. 412-417, 2015.

[17] A. E. Krasnok, A. E. Miroshnichenko, P. A. Belov and Y. S. Kivshar, «All-dielectric optical nanoantennas,» *Optics Express,* p. 20599, 2012.

[18] A. I. Kuznetsov, A. E. Miroshnichenko, M. L. Brongersma, Y. S. Kivshar and B. Luk'yanchuk, «Optically resonant dielectric nanostructures,» *Science,* p. aag2472, 2016.

[19] S. Bidault, M. Mivelle and N. Bonod, «Dielectric nanoantennas to manipulate solid-state,» *Journal of Applied Physics,* p. 126, 2019.

[20] L. Xu, G. Saerens, D. Timofeeva, D. A. Smirnova, I. Volkovskaya, M. Lysevych, R. Camacho-Morales, M. Cai, Z. K. Kamali, L. Huang, F. Karouta, H. H. Tan, C. Jagadish and A. Miroshnichenko, «Forward and Backward Switching of Nonlinear Unidirectional Emission from GaAs Nanoantennas,» *ACS Nano,* pp. 1379-1389, 2020.

[21] A. S. Shorokhov, E. V. Melik-Gaykazyan, D. A. Smirnova, B. Hopkins, K. E. Chong, D.-Y. Choi, M. R. Shcherbakov, A. E. Miroshnochenko, D. N. Neshev, A. A. Fedyanin and Y. S. Kivshar, «Multifold Enhancement of Third-Harmonic Generation in Dielectric Nanoparticles Driven by Magnetic Fano Resonances,» *Nano Letters,* pp. 4857-4861, 2016.

[22] D. Smirnova, A. I. Smirnov and Y. Kivshar, «Multipolar second-harmonic generation by Mie-resonant dielectric nanoparticles,» *Physical Review A,* p. 013807, 2018.

[23] K. Frizyuk, V. Irina, D. Smirnova, A. Poddubny and M. Petrov, «Second-harmonic generation in Mie-resonant dielectric nanoparticles made of noncentrosymmetric materials,» *Physical Review B,* p. 075425, 2019.

[24] P. Grahn, A. Shevchenko and M. Kaivola, «Electromagnetic multipole theory for optical nanomaterials,» *New Journal of Physics,* p. 093033, 2012.

[25] A. I. Kuznetsov, A. E. Miroshnichenko, Y. H. Fu, Z. JingBo and B. Luk'yanchuk, «Magnetic light,» *Scientific Reports,* pp. 1-6, 2012.

[26] M. R. Shcherbakov, D. N. Neshev, B. Hopkins, A. S. Shorokhov, I. Staude, E. V. Melik-Gaykazyan, M. Decker, A. A. Ezhov, A. E. Miroshnichenko, I. Brener, A. A. Fedyanin and Y. S. Kivshar, «Enhanced Third-Harmonic Generation in Silicon Nanoparticles Driven by Magnetic Response,» *Nano Letters,* pp. 6488-6492, 2014.

[27] T. Kaelberer, V. A. Fedotov, N. Papasimakis, D. P. Tsai and N. I. Zheludev, «Toroidal Dipolar Response in a Metamaterials,» *Science,* vol. 330, pp. 1510-1512, 2010.

[28] A. E. Miroshnichenko, A. B. Evlyukhin, Y. F. Yu, R. M. Bakker, A. Chipouline, A. I. Kuznetsov, B. Luk'yanchuk, B. N. Chichkov and Y. S. Kivshar, «Nonradiating anapole modes in dielectric nanoparticles,» *Nature Communications,* pp. 1-8, 2015.

[29] Y. Yang and S. I. Bozhevolnyi, «Nonradiating anapole states in nanophotonics: from fundamentals to applications,» *Nanotechnology,* p. 204001, 2019.

[30] L. Carletti, K. Koshelev, C. De Angelis and C. Kivshar, «Giant Nonlinear Response at the Nanoscale Driven by Bound States in the Continuum,» *Physical Review Letters,* p. 033903, 2018.

[31] V. F. Gili, L. Ghirardini, D. Rocco, G. Marino, I. Favero, I. Roland, G. Pellegrini, L. Duò, M. Finazzi, L. Carletti, A. Locatelli, A. Lemaitre, D. Neshev, C. De Angelis and Leo, G. «Metal–dielectric hybrid nanoantennas for efficient frequency conversion at the anapole mode,» *Beilstein Journal of Nanotechnology,* pp. 2306-2314, 2018.

[32] W. Fan, S. Zhang, N. Panoiu, A. Abdenour, S. Krishna, R. Osgood, K. Malloy and S. Brueck, «Second Harmonic Generation from a Nanopatterned Isotropic Nonlinear Material,» *Nano Letters,* vol. 6, pp. 1027-1030, 2006.

[33] O. Reshef, I. De Leon, Z. M. Alam and R. W. Boyd, «Nonlinear optical effects in epsilon-near-zero media,» *Nature Reviews Materials,* vol. 4, pp. 535-551, 2019.

[34] K. Pang, M. Z. Alam, Y. Zhou, C. Liu, O. Reshef, K. Manukyan, M. Voegtle, A. Pennathur, C. Tseng, X. Su, H. Song, Z. Zhao, R. Zhang, H. Song, N. Hu, A. Almaiman, J. M. Dawlaty, R. W. Boyd, M. Tur and A. E. Willner, «Adiabatic Frequency Conversion Using a Time-Varying EpsilonNear-Zero Metasurface,» *Nano Letters,* vol. 21, pp. 5907-5913, 2021.

[35] N. Zheludev and Y. Kivshar, «From metamaterials to metadevices,» *Nature Materials,* pp. 917-924, 2012.

[36] A. M. Shaltout, V. M. Shalaev and M. L. Brongersma, «Spatiotemporal light control with active metasurfaces,» *Science,* 2019.

[37] A. Nemati, Q. Wang, M. Hong and J. Teng, «Tunable and reconfigurable metasurfaces and metadevices,» *Opto-Electronic Advances,* p. 180009, 2018.

[38] S. V. Makarov, A. S. Zalogina, M. Tajik, D. A. Zuev, M. V. Rybin, A. A. Kuchmizhak, S. Juodkazis and Y. Kivshar, «Light-Induced Tuning and Reconfiguration of Nanophotonic Structures,» *Laser & Photonics Reviews,* p. 1700108, 2017.

[39] R. Paniagua-Dominguez, S. T. Ha and A. I. Kuznetsov, «Active and Tunable Nanophotonics With Dielectric Nanoantennas,» *Proceedings of the IEEE,* pp. 749-771, 2019.

[40] A. Minovich, J. Farnell, D. N. Neshev, I. McKerracher, F. Karouta, J. Tian, D. A. Powell, I. Shadrivov, H. T. Tan, C. Jagadish and Y. S. Kivshar, «Liquid crystal based nonlinear fishnet metamaterials,» *Applied Physics Letters,* p. 121113, 2012.

[41] M. Decker, C. Kremers, A. Minovich, I. Staude, A. E. Miroshnichenko, D. Chigrin, D. N. Neshev, C. Jagadish and Y. S. Kivshar, «Electro-optical switching by liquid-crystal controlled metasurfaces,» *Optics Express,* pp. 8879-8885, 2013.

[42] C. R. de Galarreeta, I. Sinev, A. M. Alexeev, P. Trofimov, K. Ladutenko, S. G.-C. Carrillo, E. Gemo, A. Baldycheva, J. Bertolotti and D. C. Wright, «Reconfigurable multilevel control of hybrid all-dielectric phase-change metasurfaces,» *Optica,* pp. 476-484, 2020.

[43] S. Makarov, S. Kudryashov, I. Mukhin, A. Mozharov, V. Milichko, A. Krasnok and P. Belov, «Tuning of Magnetic Optical Response in a Dielectric Nanoparticle by Ultrafast Photoexcitation of Dense Electron–Hole Plasma,» *Nano Letters,* pp. 6187-6192, 2015.

[44] G. P. Zograf, M. I. Petrov, D. A. Zuev, P. A. Dmitriev, V. A. Milichko, S. V. Makarov and P. A. Belov, «Resonant Nonplasmonic Nanoparticles for Efficient Temperature-Feedback Optical Heating,» *Nano Letters,* pp. 2945-2952, 2017.

[45] M. Aoussa, E. Mitsai, S. Syubaev, D. Pavlov, A. Zhizhchenko, I. Jadii, L. Hassayoun, G. Zograf, S. Makarov and A. Kuchmizhak, «Temperature-feedback direct laser reshaping of silicon nanostructures,» *Applied Physics Letters,* vol. 111, p. 243103, 2017.

[46] M. Rahmani, L. Xu, A. E. Miroshnichenko, A. Komar, R. Camacho-Morales, H. Chen, Y. Zarate, S. Kruk, G. Zhang, D. N. Neshev and Y. S. Kivshar, «Reversible Thermal Tuning of All-Dielectric Metasurfaces,» *Advanced Functional Materials,* vol. 27, p. 1700580, 2017.

[47] K. Z. Kamali, L. Xu, J. Ward, K. Wang, G. Li, A. E. Miroshnichenko, D. Neshev and M. Rahmani, «Reversible Image Contrast Manipulation with Thermally Tunable Dielectric Metasurfaces,» *Small,* vol. 15, p. 1805142, 2019.

[48] G. Marino, P. Segovia, A. V. Krasavin, P. Ginzburg, N. Olivier, G. A. Wurtz and A. V. Zayats, «Second-Harmonic Generation from Hyperbolic PlasmonicNanorod Metamaterial Slab,» *Laser and Photonics Reviews,* vol. 12, p. 1700189, 2018.

[49] R. Boyd, Nonlinear Optics, Academic Press, 2020.

[50] D. A. Smirnova, A. B. Khanikaev, L. A. Smirnov and Y. S. Kivshar, «Multipolar Third-Harmonic Generation Driven by Optically Induced Magnetic Resonances,» *ACS Photonics,* vol. 3, pp. 1468-1476, 2016.

[51] G. Marino, C. Gigli, D. Rocco, A. Lemaître, I. Favero, C. De Angelis and G. Leo, «Zero-Order Second Harmonic Generation from AlGaAs-on-Insulator Metasurfaces,» *ACS Photonics,* pp. 1226-1231, 2019.

[52] L. Wang, S. Kruk, K. Koshelev, I. Kravchenko, B. Luther-Davies and Y. Kivshar, «Nonlinear Wavefront Control with All-Dielectric Metasurfaces,» *Nano Letters,* vol. 18, pp. 3978-3984, 2018.

[53] C. Schlickriede, S. S. Kruk, L. Wang, B. Sain, Y. Kivshar and T. Zentgraf, «Nonlinear imaging with all-dielectric metasurfaces,» *Nano Letters,* vol. 20, pp. 4370-4376, 2020.

[54] Y. Gao, Y. Fan, Y. Wang, W. Yang, Q. Song and S. Xiao, «Nonlinear holographic all-dielectric metasurfaces,» *Nano Letters,* vol. 18, pp. 8054-8061, 2018.

[55] R. Grange, G. Bronstrup, M. Kiometzis, A. Sergeyev, J. Richter, C. Leiterer, W. Fritzsche, C. Gutsche, A. Lysov, W. Prost, F.-J. Tegude, T. Pertsch, A. Tunnermann and S. Christiansen, «Far-Field Imaging for Direct Visualization of Light Interferences in GaAs Nanowires,» *Nano Letters,* vol. 12, pp. 5412-5417, 2012.

[56] G. Bautista, J. Makitalo, Y. Chen, V. Dhaka, M. Grasso, L. Karvonen, H. Jiang, M. J. Huttuen, T. Huhtio, H. Lipsanen and M. Kauranen, «Second-Harmonic Generation Imaging of Semiconductor Nanowires with Focused Vector Beams,» *Nano Letters,* vol. 15, pp. 1564-1569, 2015.

[57] M. Timofeeva, A. Bouravleuv, G. Cirlin, I. Shtrom, I. Soshnikov, M. R. Escalé, A. Sergeyev and R. Grange, «Polar Second-Harmonic Imaging to Resolve Pure and Mixed Crystal Phases along GaAs Nanowires,» *Nano Letters,* vol. 16, pp. 6290-6297, 2016.

[58] S. Liu, M. B. Sinclair, S. Saravi, G. A. Keeler, Y. Yang, J. Reno, G. M. Peake, F. Setzpfandt, I. Staude, T. Pertsch and I. Brener, «Resonantly Enhanced Second-Harmonic Generation Using III–V Semiconductor All-Dielectric Metasurfaces,» *Nano Letters,* vol. 16, pp. 5426-5432, 2016.

[59] C. S. Harder, B. J. Van Zeghbroeck, M. P. Kesler, H. P. Meier, P. Vettiger, D. J. Webb and P. Wolf, «High-speed GaAs/AlGaAs optoelectronic devices for computer applications,» *IBM Journal of Research and Development,* vol. 34, pp. 568-584, 1990.

[60] K. Runge, D. Daniel, R. D. Standley, J. L. Gimlett, R. B. Nubling, R. L. Pierson, S. M. Beccue, K. C. S. N. H. Wang, M. C. F. Chang, D. M. Chen and P. M. Asbeck, «AlGaAs/GaAs HBT IC's for high-speed lightwave transmission systems,» *IEEE Journal of Solid-state circuits,* vol. 27, pp. 1332-1341, 1992.

[61] R. Chau, S. Datta and A. Majumdar, «Opportunities and challenges of III-V nanoelectronics for future high-speed, low-power logic applications,» in *IEEE Compound Semiconductor Integrated Circuit Symposium, 2005. CSIC'05.*, IEEE, 2005.

[62] S. Gehrsitz, F. K. Reinhart, C. Gourgon, N. Herres, A. Vonlanthen and H. Sigg, «The refractive index of Al x Ga 1- x As below the band gap: accurate determination and empirical modeling,» *Journal of Applied Physics,* vol. 87, pp. 7825-7837, 2000.

[63] M. Ohashi, T. Kondo, S. Fukatsu, Y. Shiraki, K. Kumata and S. Kano, «Determination of quadratic nonlinear optical coefficient of Al x Ga1- x As system by the method of reflected second harmonics,» *Journal of Applied Physics,* vol. 74, pp. 596-601, 1993.

[64] J. S. Aitchison, D. C. Hutchings, J. U. Kang, G. I. Stegeman and A. Villeneuve, «The nonlinear optical properties of AlGaAs at the half band gap,» *IEEE Journal of Quantum Electronics,* vol. 33, pp. 341-348, 1997.

[65] M. M. Fejer, S. J. B. Yoo, R. L. Byer, A. Harwit and J. S. HarrisJr, «Observation of extremely large quadratic susceptibility at 9.6--10.8 μm in electric-field-biased AlGaAs quantum wells,» *Physical Review Letters,* vol. 62, p. 1041, 1989.

[66] V. F. Gili, L. Carletti, D. Rocco, M. Finazzi, L. Ghirardini, I. Favero, C. Gomez, A. Lemaitre, M. Celebrano, C. De Angelis and G. Leo, «Monolithic AlGaAs second-harmonic nanoantennas,» *Optics Express,* vol. 24, n. 14, pp. 15965-15971, 2016.

[67] C. Gigli, G. Marino, A. Artioli, D. Rocco, C. De Angelis, J. Claudon, J.-M. Gérard and G. Leo, «Tensorial phase control in nonlinear meta-optics,» *Optica,* vol. 8, pp. 269-276, 2021.

[68] L. Carletti, A. Locatelli, O. Stepanenko, G. Leo and C. De Angelis, «Enhanced second-harmonic generation from magnetic resonance in AlGaAs nanoantennas,» *Optics Express,* vol. 23, n. 20, pp. 26544-26550, 2015.

[69] Z. Yang, P. Chak, A. D. Bristow, H. M. van Driel, R. Iyer, S. Aitchison, A. L. Smirl and J. E. Sipe, «Enhanced second-harmonic generation in AlGaAs microring resonators,» *Optics Letters,* vol. 32, n. 7, pp. 826-828, 2007.

[70] M. Celebrano, X. Wu, M. Baselli, S. Grobmann, P. Biagioni, A. Locatelli, C. De Angelis, G. Cerullo, R. Osellame, B. Hecht, L. Duò, F. Ciccacci and Finazzi, M., «Mode matching in multiresonant plasmonic nanoantennas for enhanced second harmonic generation,» *Nature Nanotechnology,* vol. 10, pp. 412-417, 2015.

[71] S. Liu, M. B. Sinclair, S. Saravi, G. A. Keeler, Y. Yang, J. Reno, G. M. Peake, F. Setzpfandt, I. Staude, T. Pertsch and I. Brener, «Resonantly Enhanced Second-Harmonic Generation Using III–V Semiconductor All-Dielectric Metasurfaces,» *Nano Letters,* vol. 16, pp. 5426-5432, 2016.

[72] D. Rocco, V. F. Gili, L. Ghirardini, L. Carletti, I. Favero, A. Locatelli, G. Marino, D. N. Neshev, M. Celebrano, M. Finazzi, G. Leo and C. De Angelis, «Tuning the second-harmonic generation in AlGaAs nanodimers via non-radiative state optimization [Invited],» *Photonics Research,* vol. 6, n. 5, pp. B6-B12, 2018.

[73] C. W. Hsu, B. Zhen, A. D. Stone, J. D. Joannopoulos and M. Soljačić, «Bound states in the continuum,» *Nature Reviews Materials,* vol. 1, pp. 1-13, 2016.

[74] M. V. Rybin, K. L. Koshelev, Z. F. Sadrieva, K. B. Samusev, A. A. Bogdanov, M. F. Limonov and Y. S. Kivshar, «High-Q Supercavity Modes in Subwavelength Dielectric Resonators,» *Physical Review Letters,* vol. 119, p. 243901, 2017.

[75] L. Carletti, D. Rocco, A. Locatelli, C. De Angelis, V. Gili, M. Ravaro, I. Favero, G. Leo, M. Finazzi, L. Ghirardini, M. Celebrano, G. Marino and A. Zayats, «Controlling second-harmonic generation at the nanoscale with monolithic AlGaAs-on-AlOx antennas,» *Nanotechnology,* vol. 28, p. 114005, 2017.

[76] J. D. Sautter, L. Xu, A. E. Miroshnichenko, M. Lysevych, I. Volkovskaya, D. A. Smirnova, R. Camacho-Morales, K. Z. Kamali, F. Karouta, K. Vora, H. H. Tan, M. Kauranen, I. Staude and C. Jagadish, «Tailoring Second-Harmonic Emission from (111)-GaAs Nanoantennas,» *Nano Letters,* vol. 19, pp. 3905-3911, 2019.

[77] D. Rocco, C. Gigli, L. Carletti, G. Marino, M. A. Vincenti, G. Leo and C. De Angelis, «Vertical Second Harmonic Generation in Asymmetric Dielectric Nanoantennas,» *IEEE Photonics Journal,* vol. 12, pp. 1-7, 2020.

[78] I. Brener, S. Liu, I. Staude, J. Valentine and C. Holloway, Dielectric metamaterials: fundamentals, designs and applications, Woodhead publishing, 2019.

[79] D. Rocco, L. Carletti, R. Caputo, M. Finazzi, M. Celebrano and C. De Angelis, «Switching the second harmonic generation by a dielectric metasurface via tunable liquid crystal,» *Optics Express,* vol. 28, pp. 12037-12046, 2020.

[80] B. Splingart, N. Tentillier, F. Huret and C. Legrand, «Liquid Crystals Applications to R.F. and Microwave Tunable Components,» *Molecular Crystals and Liquid Crystals Science and Technology. Section A. Molecular Crystals and Liquid Crystals,* vol. 368, pp. 183-190, 2001.

[81] P. Yaghmaee, O. H. Karabey, B. Bates, C. Fumeaux and R. Jakoby, «Electrically tuned microwave devices using liquid crystal technology,» *International Journal of Antennas and Propagation,* 2013.

[82] A. Komar, Z. Fang, J. Bohn, J. Sautter, M. Decker, A. Miroshnichenko, T. Pertsch, I. Brener, Y. S. Kivshar, I. Staude and D. N. Neshev, «Electrically tunable all-dielectric optical metasurfaces based on liquid crystals,» *Applied Physics Letters,* vol. 110, p. 071109, 2017.

[83] A. Komar, R. Paniagua-Dominguez, A. Miroshnichenko, Y. F. Yu, Y. S. Kivshar, A. I. Kuznetsov and D. Neshev, «Dynamic Beam Switching by Liquid Crystal Tunable Dielectric Metasurfaces,» *ACS Photonics,* vol. 5, pp. 1742-1748, 2018.

[84] M. R. Shcherbakov, P. P. Vabishchevich, A. S. Shorokhov, K. E. Chong, D.-Y. Choi, I. Staude, A. E. Miroshnichenko, D. N. Neshev, A. A. Fedyanin and Y. S. Kivshar, «Ultrafast All-Optical Switching with Magnetic Resonances in Nonlinear Dielectric Nanostructures,» *Nano Letters,* vol. 15, pp. 6985-6990, 2015.

[85] G. Grinbalt, H. Zhang, M. P. Nielsen, L. Krivitsky, R. Berté, Y. Li, B. Tilmann, E. Cortés, R. F. Oulton, A. I. Kuznetsov and S. A. Maier, «Efficient ultrafast all-optical modulation in a nonlinear crystalline gallium phosphide nanodisk at the anapole excitation,» *Science advances,* vol. 6, p. eabb3123, 2020.

[86] A. Schirato, M. Maiuri, A. Toma, S. Fugattini, R. Proietti Zaccaria, P. Laporta, P. Nordlander, G. Cerullo, A. Alabastri and Della Valle, G., «Transient optical symmetry breaking for ultrafast broadband dichroism in plasmonic metasurfaces,» *Nature Photonics,* vol. 14, pp. 723-727, 2020.

[87] M. Celebrano, D. Rocco, M. Gandolfi, A. Zilli, F. Rusconi, A. Tognazzi, A. Mazanti, L. Ghirardini, E. A. A. Pogna, L. Carletti, C. Baratto, G. Marino, C. Gigli, P. Biagioni, L. Duò, G. Cerullo, G. Leo, G. Della Valle, M. Finazzi and De Angelis, C., «Optical tuning of dielectric nanoantennas for,» *Optics Letters,* vol. 46, pp. 2453-2456, 2021.

[88] M. A. Afromowitz, «Thermal conductivity of Ga1- x Al x As alloys,» *Journal of Applied Physics,* vol. 44, pp. 1292-1294, 1973.

[89] E. R. Dobrovinskaya, L. A. Lytvynov and V. Pishchik, Sapphire: material, manufacturing, applications, Springer Science & Business Media, 2009.

[90] S. Danesi, M. Gandolfi, L. Carletti, N. Bontempi, C. De Angelis, F. Banfi and I. Alessandri, «Photo-induced heat generation in non-plasmonic nanoantennas,» *Physical Chemistry Chemical Physics,* vol. 20, pp. 15307-15315, 2018.

[91] T. Skauli, P. S. Kuo, K. L. Vodopyanov, T. J. Pinguet, O. Levi, L. A. Eyres, J. S. Harris, M. M. Fejer, B. Gerard, L. Becouarn and E. Lallier, «Improved dispersion relations for GaAs and applications to nonlinear optics,» *Journal of Applied Physics,* vol. 94, pp. 6447-6455, 2003.

[92] H. Wu, S. Pan, K. R. Poeppelmeir, H. Li, D. Jia, Z. Chen, X. Fan, Y. Yang, J. Rondinelli and H. Luo, «K3B6O10Cl: a new structure analogous to perovskite with a large second harmonic generation response and deep UV absorption edge,» *Journal of the American Chemical Society,* vol. 133, p. 7786, 2011.

[93] S. Hong, J. Dadap, N. Petrone, P. Yeh, J. Hone and J. R. Osgood, «Optical Third-Harmonic Generation in Graphene,» *Physical Review X,* vol. 3, p. 021014, 2013.

[94] A. Krasnok, M. Tymchenko and A. Alu, «Nonlinear metasurfaces: a paradigm shift in nonlinear optics,» *Materials Today,* vol. 21, p. 8, 2018.

[95] G. Naik and A. Boltasseva, «A comparative study of semiconductor-based plasmonic metamaterials,» *Metamaterials,* vol. 5, pp. 1-7, 2011.

[96] C. Simovski, P. Belov, A. Atrashchenko and Y. Kivshar, «Wire metamaterials: Physics and applications,» *Advanced Materials,* vol. 24, pp. 4229-4248, 2012.

[97] Z. Kudyshev, M. Richardson and N. Litchinitser, «Virtual hyperbolic metamaterials for manipulating radar signals in air,» *Nature Communications,* vol. 4, p. 2557, 2013.

[98] G. A. Wurtz, R. Pollard, W. Hendren, G. Wiederrecht, D. Gosztola, V. Podolskiy and A. Zayats, «Designed ultrafast optical nonlinearity in a plasmonic nanorod metamaterial enhanced by nonlocality,» *Nature Nanotechnology,* vol. 6, pp. 107-111, 2011.

[99] C. Argyropoulos, N. Estakhri, F. Monticone and A. Alu', «Negative refraction, gain and nonlinear effects in hyperbolic metamaterials,» *Optics Express,* vol. 21, pp. 15037-15047, 2013.

[100] P. Ginzburg, et al. «Manipulating polarization of light with ultrathin epsilon-near-zero metamaterials,» *Optics Express,* vol. 21, pp. 14907-14917, 2013.

[101] A. Neira, G. Wurtz, P. Ginzburg and A. Zayats, « Ultrafast all-optical modulation with hyperbolic metamaterial integrated in si photonic circuitry,» *Optics Express,* vol. 22, pp. 10987-10994, 2014.

[102] D. De Ceglia, et al. « Second-harmonic double-resonance cones in dispersive hyperbolic metamaterials,» *Physical Review B,* vol. 89, p. 075123, 2014.

[103] A. Alù, M. Silveirinha, A. Salandrino and N. Engheta, «Epsilon-near-zero metamaterials and electromagnetic sources: Tailoring the radiation phase pattern,» *Physical Review B,* vol. 75, p. 155410, 2007.

[104] M. Silveirinha and N. Engheta, «Tunneling of Electromagnetic Energy through Subwavelength Channels and Bends using ε-Near-Zero Materials,» *Physical Review Letters,* vol. 97, p. 157403, 2006.

[105] S. Campione, M. Albani and F. Capolino, «Complex modes and near-zero permittivity in 3D arrays of plasmonic nanoshells: Loss compensation using gain,» *Optical Material Express,* vol. 1, pp. 1077-1089, 2011.

[106] S. Xiao, V. Drachev, A. Kildishev, X. Ni, U. Chettiar, H.-K. Yuan and V. Shalaev, «Loss-free and active optical negative-index metamaterials,» *Nature,* vol. 466, pp. 735-738, 2010.

[107] M. Memarian and G. Eleftheriades, «Dipole radiation near anisotropic low-permittivity media,» *Progess in Electromagnetics Research,* vol. 142, pp. 437-462, 2013.

[108] A. Labelle, M. Bonifazi, Y. Tian, C. Wong, S. Hoogland, G. Favraud, G. Walters, B. Sutherland and M. Liu, «Broadband Epsilon-near-Zero Reflectors Enhance the Quantum Efficiency of Thin Solar Cells at Visible and Infrared Wavelengths,» *ACS Applied Materials & Interfaces,* vol. 9, pp. 5556-5565, 2017.

[109] Y. Tian, F. García de Arquer, C.-T. Dinh, G. Favraud, M. Bonifazi, J. Li, M. Liu, X. Zhang, X. Zheng, M. Kibria et al., «Enhanced Solar-to-Hydrogen Generation with Broadband Epsilon-Near-Zero,» *Advanced Materials,* vol. 29, p. 1701165, 2017.

[110] M. Vincenti, D. de Ceglia, A. Ciattoni and M. Scalora, «Singularity-driven second- and third-harmonic generation at ε-near-zero crossing points,» *Physical Review A,* vol. 84, p. 063826, 2010.

[111] A. Ciattoni, C. Rizza and E. Palange, «Extreme nonlinear electrodynamics in metamaterials with very small linear dielectric permittivity,» *Physical Review A,* vol. 81, p. 043839, 2010.

[112] M. Vincenti, M. Kamandi, D. de Ceglia, C. Guclu, M. Scalora and F. Capolino, «Second-harmonic generation in longitudinal epsilon-near-zero materials,» *Physical Review B,* vol. 96, p. 045438, 2017.

[113] X. Wen, G. Li, C. Gu, J. Zhao, S. Wang, C. Jiang, S. Palomba, C. de Sterke and Q. Xiong, «Doubly Enhanced Second Harmonic Generation through Structural and Epsilon-near-Zero Resonances in TiN Nanostructures,» *ACS Photonics,* vol. 5, pp. 2087-2093, 2018.

[114] M. Alam, S. Schulz, J. Upham, I. De Leon and R. Boyd, «Large optical nonlinearity of nanoantennas coupled to an epsilon-near-zero material,» *Nature Photonics,* vol. 12, p. 79, 2018.

[115] D. Rocco, M. A. Vincenti and C. De Angelis, «Boosting Second Harmonic Radiation from AlGaAs Nanoantennas with Epsilon-Near-Zero Materials,» *Applied Sciences,* vol. 11, p. 2212, 2018.

[116] D. Rocco, C. De Angelis, D. De Ceglia, L. Carletti, M. Scalora and M. A. Vincenti, «Dielectric nanoantennas on epsilon-near-zero substrates: Impact of losses on second order nonlinear processes,» *Optics Communications,* vol. 456, p. 124570, 2020.

[117] K. Koshelev, S. Kruk, E. Melik-Gaykazyan, J.-H. Choi, A. Bogdanov, H.-G. Park and Y. Kivshar, «Subwavelength dielectric resonators for nonlinear nanophotonics,» *Science,* vol. 367, pp. 288-292, 2020.

[118] E. Melik-gaykazyan, K. Koshelev, J. Choi, S. Kruk, A. Bogdanov, H. Park and Y. Kivshar, «From Fano to quasi-BIC resonances in individual dielectric nanoantennas,» *Nano Letters,* vol. 21, pp. 1765-1771, 2021.

[119] Z. Liu, Y. Xu, Y. Lin, J. Xiang, T. Feng, Q. Cao, J. Li, S. Lan and J. Liu, «High-Q quasibound states in the continuum for nonlinear metasurfaces,» *Physical Review Letters,* vol. 123, p. 253901, 2019.

[120] V. Zubyuk, L. Carletti, M. Shcherbakov and S. Krul, «Resonant dielectric metasurfaces in strong optical fields,» *APL Materials,* vol. 9, p. 060701, 2021.

[121] L. Carletti, S. S. Kruk, A. A. Bogdanov, C. De Angelis and Y. Kivshar, «High-harmonic generation at the nanoscale boosted by bound states in the continuum,» *Physical Review Research,* vol. 1, p. 023016, 2019.

[122] E. A. A. Pogna, M. Celebrano, A. Mazzanti, L. Ghirardini, L. Carletti, G. Marino, A. Schirato, D. Viola, P. Laporta, C. De Angelis, G. Leo, G. Cerullo, M. Finazzi and G. Della Valle, «Ultrafast, All Optically Reconfigurable, Nonlinear Nanoantenna,» *ACS Nano,* vol. 15, pp. 11150-11157, 2021.